参赛队员姓名：熊竑奕

中学：Shenzhen College of International Education

省份：广东

国家/地区：中国

指导教师姓名：姜鹏

指导教师单位：中国极地研究中心

论文题目：Morphology of Broad Emission Lines from Binary Supermassive Blackholes

Artist's Impression of Blackholes in Binary Motion

Morphology of Broad Emission Lines from Binary Supermassive Blackholes

Hongyi Xiong

Abstract:

The 2020 Nobel Physics Prize was awarded for the study of black holes. Dr. Roger Penrose proved that blackholes are a robust consequence of general relativity, Dr. Andrea Ghez and Reinhard Genzel verified the existence of a supermassive object at the center of the milky way. It is widely believed that every galaxy hosts a supermassive black hole at its center. The interaction between galaxies and their supermassive blackholes plays an important role in the evolution of galaxies. Galaxy mergers are commonly seen in the universe, so it is also expected to detect the mergers of supermassive blackholes. Prior to blackhole mergers, two supermassive blackholes undergo a "binary stage" in Keplerian orbit, while the orbit gradually decays and eventually merges. Binary supermassive blackholes are an important stage in evolution of galaxies. However, the extremely long timescale of observation limits the actual number of binary blackholes identified by their Keplerian motion, as their period usually ranges up to decades, if not centuries. The other difficulty is that most supermassive blackholes are silent, almost undetectable. However, when large amounts of gases begin to accrete on to the central blackhole it can become active, turning into the most luminous objects in the universe, known as Active Galactic Nuclei. Binary forming by two active supermassive black holes is much easier for observing. In this paper, we studied the feasibility of identifying binary active black holes from spectroscopy.

Accretion onto a blackhole can induce extreme radiation stimulating emission lines in nearby gases. In the deep gravitational well, these clouds move at speeds up to 5000 km/s, and so broadens the emission lines via the Doppler Effect. These broad emission lines are known as broad-lines, present on spectra of AGNs. The line-emitting region where such emission lines are produced is known as the broad-line region (BLR). We developed a self-consistent model to describe both the geometrical shape of the BLR and the dynamics of the gas clouds in the BLR. The motion of clouds is described by a series of Keplerian orbits. The spectral shift of emission line can be derived by the radial velocity at each point in Keplerian orbits. Assuming that the BLR is stable, that is, the structure and distribution of gas in BLR doesn't change over a considerable period of time, the accumulated emission line profile can be constructed by simple addition of all Keplerian orbits in the BLR. By comparing the calculated profiles to spectra observed in SDSS (Sloan Digital Sky Survey), we found that our model can satisfactorily match most observed profiles.

We applied the model with modification to the study of binary AGNs and their profiles of emission lines. We considered the velocity offset due to binary motion and

added their respective profiles to produce the final, resulting binary profile. Three kinds of emission line profiles are featured as binary AGNs in our simulations: twin-peak structures where two strong broad-lines are present; sub-peak structures where a smaller but still visible emission line accompanies the dominant line; velocity offset structures where the single emission peak visible is displaced from the center-of-mass redshift derived from the redshift of thin emission-lines. We then analyzed 1348 AGN spectra with high S/N ratio in SDSS database, and selected 26 as candidate binary supermassive blackhole systems. These candidates are valuable for following-up observation, their binary nature could be confirmed by detecting the profile variation due to orbital motions.

Key words: Binary systems, Supermassive blackholes, AGN, broad-emission lines, emission profile

Contents

1 INTRODUCTION

1.1 Blackholes in Theory

In the 1910s Einstein established the theory of general relativity. In Einstein's theory, the properties of space-time govern the motion of matters, and the distribution of matters curve space-time, quantitively described in Einstein's Field equations. Months after the introduction of General Relativity, Karl Schwarzschild found a solution to the equations by assuming perfect spherical symmetry, best known as the *Schwarzschild Metrics*:

$$ds^2 = \left(1 - \frac{r_s}{r}\right) c^2 dt^2 - \left(1 - \frac{r_s}{r}\right)^{-1} dr^2 - r^2 d\theta^2 - r^2 \sin^2\theta \, d\phi^2 \quad (1.1)$$

Where r_s is the Schwarzschild radius, given by $r_s = \frac{2GM}{c^2}$, defining the magnitude of the event horizon of the black-hole. Any information inside the event horizon cannot transmit crossthe Schwarzschild radius.

Schwarzschild's solution, as well as a later solution known as the Kerr metrics (rotating black hole), were all based on symmetries and assumed perfection. Nature yielded nothing perfect, so it was wondered whether blackholes could exist in real universe, if not for the perfect conditions (either spherical or cylindrical symmetry) as the solutions asked for.

In the 1970s Dr. Roger Penrose, using ideas of "trapped surfaces", proved that blackholes are in fact a robust consequence of general relativity itself, demonstrating general existence of blackholes. The 2020 Nobel Physics prize was awarded to R. Penrose "for the discovery that black hole formation is a robust prediction of the general theory of relativity (*2020 Nobel Physics*)." In the darkness of space there are now more of those "dark stars" than we realize. If blackholes are to be commonly occurring in the universe, its role must be significant in the growth and development of the universe. The Milky Way itself hosts a supermassive blackhole at its very center, the discovery sharing the 2020 Nobel Physics prize. It is now in fact believed that blackholes, being a common occurrence in the universe, were at the center of every galaxy.

1.2 Blackholes in Observation

Blackholes can be distinctly classified into two classes according to their masses. Stellar mass blackholes are quite known for some time, its formation widely believed to be from the collapse of giant stars. The other, supermassive blackholes, ranges from millions to billions of solar masses, and are now commonly accepted commonly existing at the center of all galaxies. Indirect evidence led by Reinhard Genzel and Andrea Ghez to reveal a supermassive blackhole at the center of our galaxy, in the sight of view to Sagittarius A*. The close orbits of the stars near the Galactic center enables measurement of the center mass which they orbiting around. Most noticeably for the star S2, has a period of less than 16 years, with an extremely high orbital eccentricity at 0.88 (Ghez at al., Gillessen et al.). All orbital measurements yield a massively compact object with 4 million solar masses (Ghez at al., Gillessen et al.). Even more recent imaging using VLBI (Very Long Baseline Interferometry) technique by the EHT (Event Horizon Telescope) identified the radiation from the *innermost stable circular orbit,* $r_{ISCO} = 3R_s$ of the blackhole at the center of M87 (See **Fig. 1**)

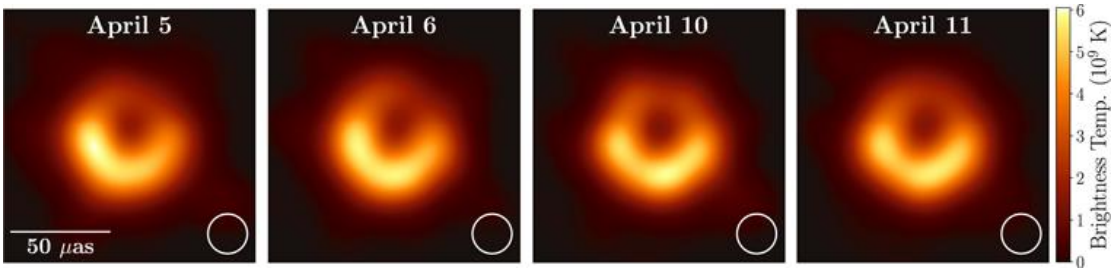

Fig. 1 Image of the blackhole M87 taken by the EHT. The four images are computed as an average of a collection of images taken. Credit: The Event Horizon Telescope Collaboration, Akiyama et al. (2019)

Direct observations of supermassive blackholes require said subjects to be *active*, that is, outputting astounding amounts of luminosity to be observed at far enough distances. In fact, they are first associated with *quasi-stellar* objects, or QSO, as compact radio sources. In the 1960s Maarten Schmidt identified QSO 3C 273 as an extragalactic source with redshift 0.158. He soon identified several others, with redshifts ranging up to $z > 2$. Schmidt summarized several properties, including large UV fluxes (UV excess), time-varying continuum flux, and broad emission lines (e.g., see **Fig. 2**) which now constitute the prominent features of AGNs, or Active Galactic Nuclei. Now there are about one million known AGNs.

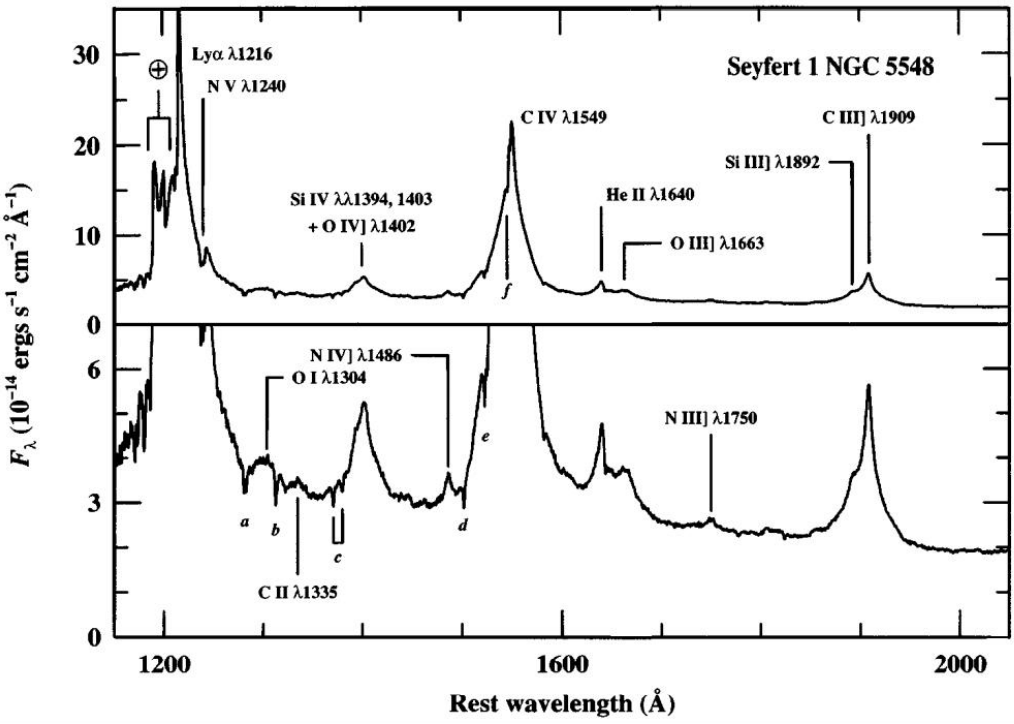

Fig. 2 Ultraviolet spectrum of NGC 5548. Broad features of the emission lines are typical to AGNs of the Seyfert 1 class. Notable broad emission lines include $C\ IV\ \lambda 1549$, and the Balmer lines in the visible (or infrared) region. Power-law spectrum identified with synchrotron radiation. Credit: Faint Object Spectrograph, Hubble Space Telescope (HST)

1.3 Active Galactic Nuclei

The cores of AGN are thought to be unusually compact. This is evident from the unresolved core at the highest possible resolution by the Hubble Space Telescope (HST). This, along with the high luminosity at $\sim 10^{47}\ erg\ s^{-1}$, suggests an extremely massive (and compact) object so its luminosity would not exceed the Eddington Limit, by considering the equilibrium between gravitational force and radiation pressure:

$$L_E = \frac{4\pi cGMm_p}{\sigma_T} = 1.3 \times 10^{38} \frac{M}{M_{sun}}\ erg\ s^{-1} \quad (1.2)$$

To radiate at the Eddington Luminosity requires a mass of $\sim 10^9 M_{sun}$, precisely the mass expected at the center of most galaxies. Energy generation mechanism for AGNs are thought to be in the form of accretion, onto a supermassive blackhole. The luminosity is defined by $L = \eta \dot{M} c^2$, where $\dot{M}$ is the *mass accretion rate* and η the hypothesized mass efficiency. For AGNs continuously radiating for $3 \times 10^7 yr$, the mass efficiency must be of order ~0.1. For a supermassive blackhole, accretion onto the blackhole requires an object falling to the innermost stable circular orbit at $3R_s$. This process radiates half of the energy away as thermal radiation by the virial theorem. Thus, the luminosity can be written as:

$$L = \frac{GM\dot{M}}{2r_{ISCO}} = \frac{GM\dot{M}}{12GM/c^2} = \frac{1}{12}\dot{M}c^2 \quad (1.3)$$

Where $\eta \sim 0.083$, of the right order of magnitude. Using the correct relativistic potential and energy gives $\eta \sim 0.057$. For comparison, fusion reactions inside stars are of an order of magnitude less than accretion efficiencies. In order to verify the possibility of accretion as an energy generation mechanism, we define the *Eddington Accretion Rate*, the maximum accretion rate that the AGN can sustain, to be $\dot{M}_E = \frac{L_E}{\eta c^2} = 4 \times 10^{-8} M_{sun}\ yr^{-1} \frac{M}{M_{sun}}$. For a typical $10^9 M_{sun}$ this would require an accretion rate of 40 solar masses per year. The mass requirements of accretion are then generally considered to be irrelevant; a 40 solar masses per year is insignificant compared to most supermassive objects at the center of galaxies.

Observed AGNs show a wide variety of features, particularly in the optical spectrum. Differing features exists in observed AGNs allows classification into categories. Typically, there exists two types of classes initially selected for their radio-loud properties, with magnitude $M_B > -21.5 + \log h_0$, Seyfert II AGNs differ from Seyfert Is in that there are no broad emission lines present in their spectra. The assumption that there is in fact little variation in AGN structure led to the proposal of the *Unified Model*, where Seyfert Is and Seyfert IIs occur as a result of different orientation angle in the celestial plane (See **Fig. 3**). Osterbrock (1978) firstly suggested that conventional models give a high degree of anisotropy and the importance of orientations in observing AGNs. The weaker continuum of Seyfert IIs can be explained by ring-like dust torus obscuring the broad components of emission lines in the central region; whereas in Seyfert Is, the orientation is almost face-on and the broad emission lines are present. The model suggests that the "gas torus" surrounds the central emission region, including the broad-line region (BLR), at a distance 50pc~100pc. Additionally, the narrow-line region (NLR) lies outside this torus and so is present in Seyfert I and Seyfert II. Further evidence points to that the space density of observed Seyfert IIs are 3 times more numerous than Seyfert Is (Peterson, *Introduction to Active Galactic Nuclei*), in accordance with the fact that isotopically distributed orientation angles prefer a higher inclination (as edge-on).

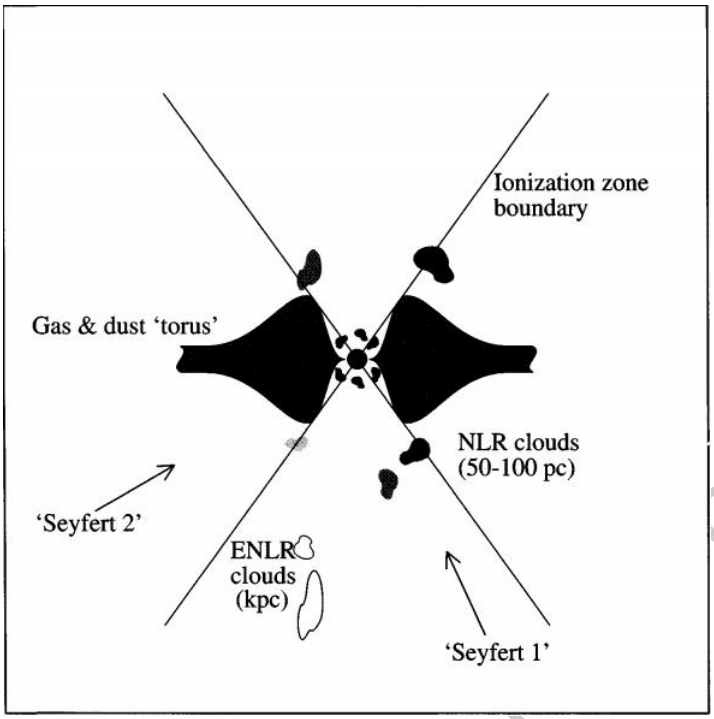

Fig. 3 Simplified unification model. BLR clouds lie in the central region, surrounded by a "dust torus" at distances of pc. NLR clouds lie at kpc distance and so is not extinguished in neither Seyfert Is and IIs. Credit: Introduction to Active Galactic Nuclei, Peterson

1.4 Binary Blackholes

The sufficiently high mass-energy efficiency implies that only a relatively low mass accretion rate is required for generating such high luminosities. However, the accretion disk component ranges to approximately the order of light-days, so that angular momentum considerations will affect accretion rates. For gases at distances 10kpc, falling sufficiently close to the blackhole, i.e., ~0.01pc, where friction and viscosity can become important, requires only 10^{-5} of the initial angular momentum per mass (see *Peterson, Introduction to AGN*). Such loss can be greatly explained by tidal force between interacting binaries, or binary blackholes. Strong gravitation interaction between galaxies at sufficiently close distances can remove angular momentum for accretion to occur. Binary blackholes could be important mechanism for accretion and growth of supermassive blackholes.

Hence, the study of binary AGN systems can greatly improve our understanding of the nature of such luminous objects, and how they came to become active, as well as the evolution of galaxies. Such targets are relatively rare as their short duty cycle in the evolution of blackholes, and much more common are those following Keplerian orbits, i.e., gravitationally bound but far enough to neglect effects of general relativity. Such AGN systems are studied via optical methods, by observing their emission spectra. Prominent features in AGN spectra are the doppler-broadened lines, particularly the Balmer lines. The identification of broad lines is thus important in identifying AGNs.

However, there is a lack of knowledge over the true structure of the BLR region; not much

known is about is geometry shape nor its dynamical nature. This is because the BLR regions in distance AGNs cannot be spatial resolved. Reverberation techniques (Peterson et al.) identifies a strong response of the BLR from continuum flux, suggesting optically thick clouds and a BLR size of about 10 light-days. Attempts have been made to identify spectra unique to binary sources, most notably by Boroson & Lauer (2009). They identified the source J1536+0441 (See **Fig. 4**) as a binary blackhole at separation ~0.1 pc, and velocity separation 3500 km/s. Emission spectra demonstrated binary peak systems in all Balmer broadlines, with redshifts z = 0.3889 and z = 0.3727, respectively, the red and blue system, a clear evidence of the superimposing nature of binary blackholes. Different interpretation exists, however. Zhang et al. (2019) interpreted J1536+0441 as a single blackhole due to the lack of the blue system at the He I and the Paschen lines. The model suggested that a shocked flow is responsible for the emergence of double emission lines. Hence, great uncertainty lays in the spectra of binary systems and it is this difficulty that allows us only to select possible *candidates.* In addition, double peaked structures have been reportedly been identified in single-blackhole systems, for example NGC 1097 where a broad, double peaked component is seen alongside a superimposed BLR. Storchi-Bergmann et al. (2017) suggested that this is a signature of accretion disk emission, arising from its outer part.

Although extensive work and research has been developed towards identifying binary blackhole systems, difficulty remains in describing fully the wide range of variability existing in observed systems. The lack of knowledge about the physical nature of the BLR permits us only to rely on model-based assumptions, developing theoretical profiles to fit observed broad-lines.

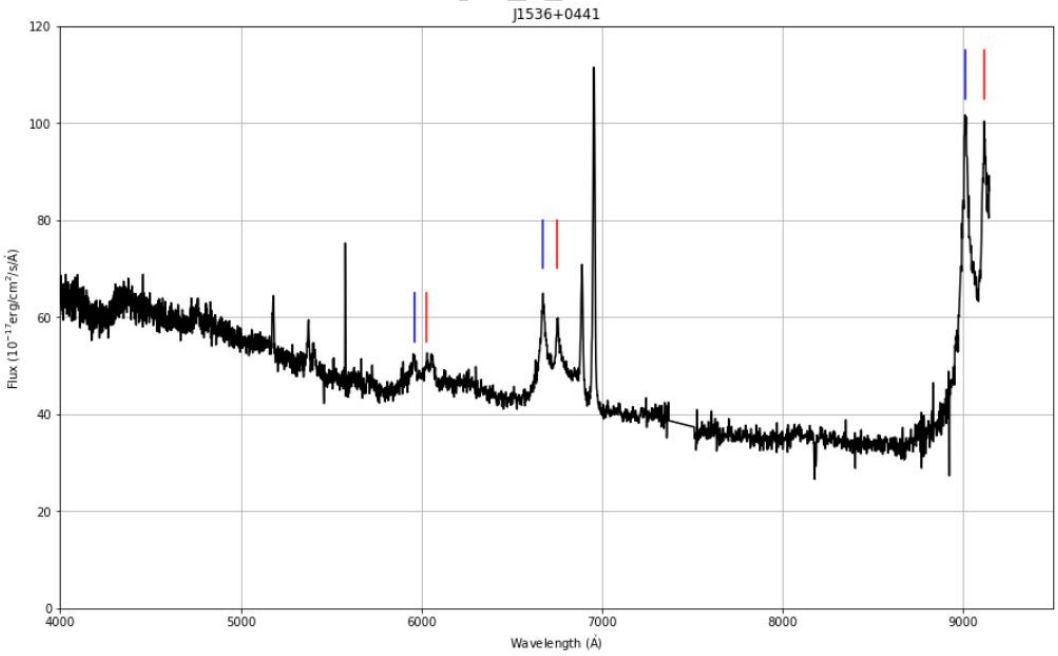

Fig. 4 SDSS spectra of J1536+0441.The marked lines indicate the $H\gamma$,$H\beta$, and $H\alpha$ systems. Blue line indicates the lower redshift system z = 0.3727, and the red lines indicate the higher redshift system, z = 0.3889. Double peaked narrow lines are the $O_{III]}$ λ5007 and $O_{III]}$ λ4959, at a similar redshift to the red system. Boroson et al. identified the binaries to be at a distance 0.1 pc, and thus would share the NLR region.

Some binary systems, too, have been identified with single emission lines that displays no

apparent difference to the spectra of single blackholes, but their periodic variation of brightness. Graham et al. (2015) identified the periodic optical variation in the AGN PG1302-102, whose spectrograph (emission lines) displays no apparent difference to that of single AGNs. Skewed lines from their center-of-mass redshifts were also observed in binary candidates, for example J001224 (Eracleous et al. 2012), in which the peak is shifted by 90 $km\ s^{-1}$ relative to the narrow line redshift (the O III lines). This is thought to arise from the weaker nuclear activity of its binary counterpart, erasing the additional set of lines.

Overall, although broad-lines are prominent features to AGN spectra, their profile structure in binary systems remains unclear and unpredictable. It would therefore be of interest to be able to summarize relevant patterns and structures in binary spectra, selecting them from AGN spectra.

2 MODEL THEORY

2.1 Kepler's Laws

Non-relativistic objects are governed by Kepler's laws. The BLR regions are thought to be far enough (~50 light-days) from the central blackhole so that Newtonian gravity completely dominates and Kepler's laws apply. In our simplified model the BLR gas are completely under the influence of gravity, performing bound orbits. Furthermore, strong responses from the emission lines to continuum variability suggests an optically-thick medium, and Peterson (1993) suggested that the "cloud-covering factor" is small. In our simplified model, we can then neglect effects of obscuring by clouds in the BLR, and instead rely purely on Keplerian motion. This allows a simple construction of Keplerian orbits for the BLR clouds.

In space, a Kepler orbit is described by a set of chosen parameters: a, the semi-major axis of an elliptical orbit; e, the eccentricity of the orbit; P, the period of the orbit. In addition to this, the inclination, i, is used to describe the orientation of the orbit relative to the sky plane. Finally, ω is used to describe the position of the *pericenter*, called the argument of pericenter. These parameters specify the shape of the object's orbit under gravitational influence (See **Fig. 5**), as well as its orientation In addition, Kepler's Laws can be described as the following:

1. Motions under gravity follow conic paths; in bound scenarios, this refers to elliptical orbits.
$$r = \frac{a(1-e^2)}{1+e\cos\nu} \quad (2.1)$$
The quantity ν is defined as the objects position in angular coordinates (see **Fig. 5**)
2. Orbiting objects sweep out equal areas in equal time. This is a statement of angular momentum conservation:
$$\frac{dA}{dt} = \frac{1}{2}r^2\dot{\theta} = Constant$$
3. The square of the period is proportional to the third power of the semi-major axis of the orbit.
$$\left(\frac{P_1}{P_2}\right)^2 = \left(\frac{a_1}{a_2}\right)^3$$
This relationship holds for all objects under the same gravitational influence. The period and the semi-major axis can be explicitly determined by the following equation:
$$P^2 = \frac{4\pi^2 a^3}{GM}$$
The mass M takes on different expressions for different orbits of interest. However, as the

mass of the total BLR is significantly smaller than that of the central blackhole, we can safely assume that M is simply the mass of the blackhole.

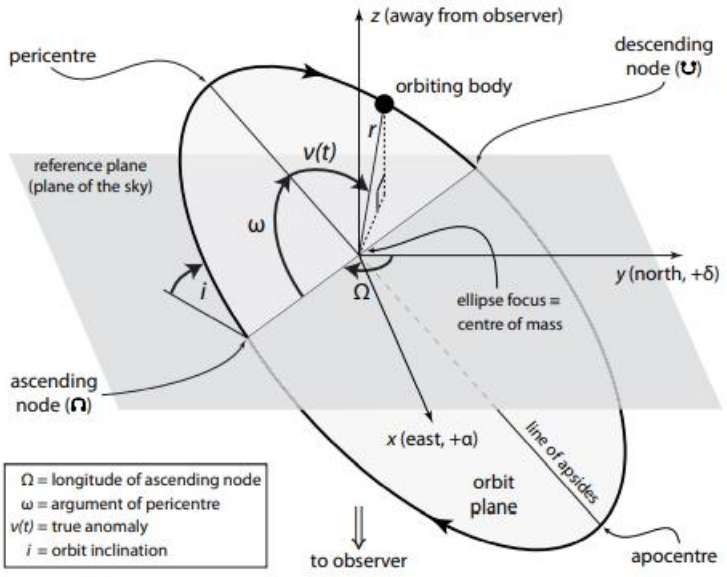

Fig. 5 Diagram of orbit in space. Note the inclination is measured relative to the plane of the sky. $v(t)$ is the *true anomaly*, the angular position of the orbiting body on the orbit. Credit: The Exoplanet Handbook, Chapter 2

2.2 Radial Velocity

Doppler-broadened broad-lines in spectra profiles are a prominent feature of AGNs (Seyfert Is). Doppler shifts arise from the differing *radial velocity* of the broadline clouds at different parts of the orbit. *Redshifts* occur when the line-of-sight velocity is pointing away from the observer, and *blueshifts* occur when the line-of-sight velocity is pointing towards the observer. On different sections of the elliptical orbit the redshift is seen by different amounts, and so hence one orbit necessarily covers a wide range of velocities.

The *radial velocity semi-amplitude* is derived as:

$$K = \frac{2\pi}{P}\frac{a \sin i}{\sqrt{1-e^2}}$$

Then the radial velocity equation can be expressed as:

$$v_r = K(\cos(\omega + v(t)) + e\cos\omega) \quad (2.2)$$

Where v is the true anomaly of the orbiting body (See **Fig. 5**), as a function of time.

2.3 Profile of Broad Emission lines

The line profile can be conveniently expressed in *velocity space,* where the axis is labeled in velocity units. The broadline profile is then equivalent to the velocity distribution; areas where a velocity occurs the most contributes the most amount of flux to the profile. In practice, spectrograph resolution cannot be infinitely large, for our interest we take the "resolution" to be ~50 km/s (almost the same resolution of SDSS surveys). That is, we will sample at 50 km/s intervals over the entire orbit for BLR clouds.

For simplicity, our geometric model will assume the following:

1. Mass continuity of the BLR clouds. Although the BLR clouds are assumed to be sparse and

non-obscuring, the individual clouds are fast enough in orbit to allow the assumption of mass continuity: At any given point on the orbit the rate of the mass of the clouds entering is equal to the rate at which the clouds are leaving. This allows us to ensure that every velocity sample is occupied by BLR clouds. This assumption is evident from the observed variation of BLR spectra (time taken for the profile to change significantly), which is at the order of ~10 years. With such a long variation timescale, the stability of the orbit is ensured, thus allowing us to find the distribution of clouds, treating it as a continuous element.

Although the true distribution, the distribution of clouds following the true anomaly, is unknown and complicated for eccentric orbits, BLR clouds are evenly distributed on the *Mean anomaly*, represented by $M(t) = \frac{2\pi}{P}(t - t_p)$, where t_p is a time normalization constant.

In particular, the mean anomaly is related to the *Eccentric anomaly* and the true anomaly (see **Fig. 6**) by the following equations:

$$M(t) = E(t) - e \sin E(t) \quad (2.3)$$

$$\cos v(t) = \frac{\cos E(t) - e}{1 - e \cos E(t)} \quad (2.4)$$

In practice to locate the position of an object (usually done for satellites and exoplanets), equation (2.3) and (2.4) needs to be solved numerically. However, the linear relationship between time and the mean anomaly is sufficient for our uses. Specifically, we assume that the mass distribution is linear with time. For where Δt is large, we expect a larger proportion of BLR clouds and hence contributing more flux to the profile.

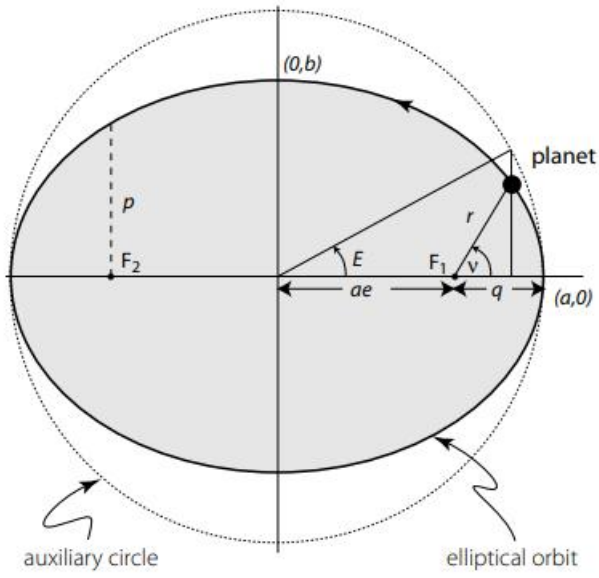

Fig. 6 The Eccentric anomaly and the true anomaly. The mean anomaly is defined as the angle the planet would travel (in the same time) on the ellipse's auxiliary circle. Credit: The Exoplanet Handbook, Chapter 2

The simple relation between time intervals and mass allows us to be able to directly derive the line profile from a radial velocity curve, as the time intervals corresponding to a specific velocity interval is proportional to the mass of BLR clouds at that interval. This will be described in detail in section **2.4**.

2. In addition, we assume a simple relationship, in the form of a power law, for the radial emission capabilities. It is clear that the emission capability of an orbit with semi-major axis

a must depend on the volume (mass) of gas radiating and the intensity of light reaching the BLR clouds from accretion emission. In a simplified model the space density of BLR mass can be taken to be constant. In this case the mass of the BLR scales as a linear function of the semi-major axis. In addition, photonization power from the central blackhole drops as $\sim r^{-2}$, so we expect an inverse relationship. We can then write the *radial weight* as:

$$W_R(a) = a^{\gamma}, \ \gamma \leq 0 \qquad (2.5)$$

Equation 2.5 constrains the possible values of the parameter γ: The weight must decrease as the semi-major axis increases; it is physically not possible for the emission capabilities to increase further out into the BLR region.

3. Emission capabilities must also be taken into account from the angular distribution of clouds. Orbiting bodies at the equatorial plane (of the central blackhole) are expected to have a greater emission capability than those whose orbits are at the face-on configuration. This is mainly due to the rotation of the blackhole; gas particles entering the BLR are likely to be found near the equatorial plane of the blackhole. Similarly, radiation from the accretion disk lie primarily on the equatorial plane. Thus, we expect a greater fraction of contribution from BLR orbits whose inclination are close to that of the blackhole inclination. This can be described using a cosine-power law.

$$W_{\theta}(i) = \cos^{\beta}(i - \theta_{inc}) \qquad (2.6)$$

It should be noted that in (2.6) the inclination of the central blackhole must not exceed a certain limit. The unification model (**Fig. 3**) suggests that broadlines are present in Seyfert Is, whose orbital inclinations are low (i.e., face on)

The sum of all contributions from every BLR orbit constitute the broad line profile. Once the flux contribution from all orbits is known, each Kepler orbit is given an appropriate weight depending on the orbit's inclination and the semi-major axis.

2.4 Constructing Broadline profiles

2.4.1 Method of construction

The relation between time interval and BLR mass is established in section **2.3**. The generation of radial velocity curves based on the Keplerian parameters is tedious analytically, but numerical solutions can be easily computed with computing power. In our model we use the module *Radvel* calculates a radial velocity curve for one period of BLR motion. *Radvel* generates a radial velocity curve given the parameters (K, P, e, ω, t_p), where t_p is a time correction constant we take to be 0. Note that although the Keplerian orbit is also described by the central mass, inclination, and semi-major axis, these are embedded in K and P, related via Kepler's third law. In practice, *Radvel* takes in $(K, P, e\cos\omega, e\sin\omega, t_p)$. To calculate the distribution, or flux contribution, of each velocity interval requires sampling from the radial velocity curve to create a histogram. This is done by taking samples of 50 km/s, corresponding to the resolution of SDSS spectrographs, and noting the time interval the BLR clouds had spent on that velocity interval (see **Fig. 7**). Following the discussion from section **2.3**, this is equivalent to the relative flux that given velocity contributes, and hence the resulting profile for a single orbit is a histogram of the "relative frequency" of velocity.

Construction of the BLR region in 3-D requires our model to run over radial and angular directions. We define an opening angle, θ_{open}, to describe the range of values the inclination can take. With $\theta_{open} = 90°$, this corresponds to a completely spherical BLR.

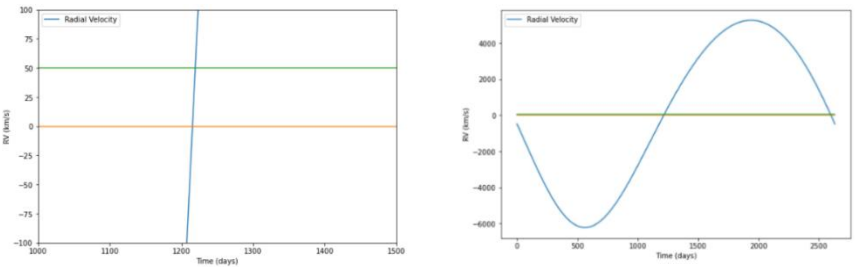

Fig. 7 Sampling the radial velocity curve. The blue line indicates the radial velocity curve for one period of orbit. The green and orange lines indicate a velocity interval of 50 km/s. The interval of time corresponding to the section of the curve in the velocity interval is directly associated with its emission capability.

Thus, to construct the model for the full BLR region, we must first create the flux profile for a single orbit. We then must let the geometry parameters, namely the semi-major axis and the inclination, run over the entire allowed region, defined by the opening angle and the inner & outer radius. The final profile is constructed by giving appropriate weight to each of the single-orbit profiles, described by a power law and a cosine-power relation. Finally, we consider effects of the turbulent velocity (*Pancoast et al. 2014*), described by a Lorentz function $f(v) = \frac{1}{\pi}\left(\frac{v_t}{v^2+v_t^2}\right)$, where v_t is the turbulent velocity, usually of the order ~500 km/s, sometimes ranging up to 1000 km/s, and thus having a profound effect on the profile. The effect of turbulent velocity is one of convolution; that is the profile is given by the convolution of the (original) line profile with $f(v)$

Parameter	Value	Description
$\mathbf{a_{in}}$	$10\sim20\ ltd$	Inner radius (semi-major axis)
$\mathbf{a_{out}}$	$20\sim100\ ltd$	Outer radius (semi-major axis)
$\boldsymbol{\theta_{inc}}$	$0°\sim30°$	Viewing angle of BLR
$\boldsymbol{\theta_{open}}$	$0°\sim90°$	Opening angle of BLR
$\mathbf{e}$	$0\sim1$	Overall eccentricity of orbit
$\boldsymbol{\omega}$	$0°\sim180°$	Overall argument of pericenter
$\boldsymbol{\gamma}$	$-2\sim2$	Radial weight
$\boldsymbol{\beta}$	$0\sim7$	Angular weight
$\mathbf{v_{turb}}$	$500\sim1000\ km/s$	Turbulent velocity
$\mathbf{M_{B,1}}$	$10^{8\pm1}M_{sun}$	Blackhole mass
$\mathbf{M_{B,2}}$	$10^{8\pm1}M_{sun}$	Blackhole mass
$\boldsymbol{\eta_1}$	$0\sim0.1$	Mass accretion rate
$\boldsymbol{\eta_2}$	$0\sim0.1$	Mass accretion rate
$\mathbf{r}$	\	Separation of binary cores

Table 1. List of model parameters. It must be noted that the eccentricity is described to reflect the overall asymmetry of the BLR region, not of a particular single orbit.

2.4.2 Binary profiles & Double peaked single AGNs

Construction of the binary profile at its core can be taken to be a simple addition of fluxes. Factors that must be taken into consideration are 1. The radial velocity separation of the respective binary cores, calculated from the mass ratios given by $v_1 = \frac{2\pi}{P}\frac{1}{1+r}a\sin i\ (\cos(\omega+\nu)+e\cos\omega)$ and $v_2 = \frac{2\pi}{P}\frac{r}{1+r}a\sin i\ (\cos(\omega+\nu)+e\cos\omega)$, where the ratio r is the ratio of blackhole masses:

$r = \frac{M_{B,1}}{M_{B,2}}$; and 2. The luminosity ratios which determines the relative contributions from each core to the final profile. An important assumption here is that there is no apparent difference in the self-emission capabilities of the BLR clouds of the two AGNs; their brightness ratio is solely determined by the property of the blackhole itself. Observations and reverberation mappings (*Introduction to Galactic Nuclei, 5.5*) suggests a strong relation between continuum flux and broadline profile; the continuum flux in turn is determined by blackhole accretion rates, as well as the mass of the central blackhole. Thus, in a simplified model, the "brightness" of a broadline profile can be described as the product of blackhole mass and accretion rate. Thus, the brightness ratio, b, is described as $b = \frac{M_{B,1}\eta_1}{M_{B,2}\eta_2} = r\frac{\eta_1}{\eta_2}$. In particular, if one of the blackhole is not accreting, i.e., no broadline, then$\eta_1 = 0$ and the ratio is 0. Note that the order of indices is not relevant.

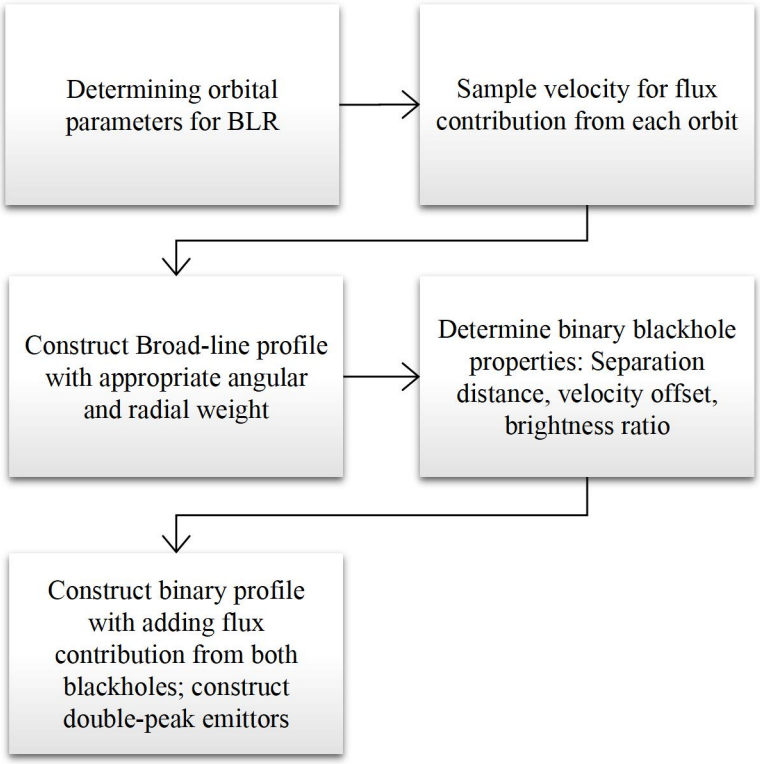

Fig. 8 Diagram of modelling process. Selection of orbital parameters will generally be used to determine effects of various parameters on the profile. This constricts the possible values for constructing the true binary profile

The velocity separation calculated above is relative to the *center of mass*, determined by the redshift of the narrow line region (NLR), most prominent of those the O[III] lines. This is because as both cores not being far apart, share the NLR region (X.-W. Wang and H.-Y Zhou), and so the velocities represent each cores redshift from its center of mass.

Another result we wish to reconstruct in our model are the double-peak emitters from single AGNs. In such a scenario, model construction requires two steps: The determination of parameters for the broadline, and for the outer edge of the accretion disk. Note that however the viewing angle must not be changed for both steps; they are part of a single blackhole system. The selection of parameters requires strict constriction: one, the inclination must not exceed a certain limit,

beyond which broadlines should disappear by the Unified model (**Section 1**). Two, the conditions for the broad, double-peak component requires a small inner and outermost radius, and that its inclination must be the same as the broadline component. Finally, we must appropriately weigh each component flux, for accretion disk radiation would be expected to be dominant at this stage. Overall, the steps in **Fig. 8** describe the process we will follow to construct broadline profiles for single AGN and binary AGNs.

3 SIMULATIONS AND OBSERVATIONS

3.1 Single AGN Emission Lines

3.1.1 Disk-Like BLR

Disk-like BLR models the whole of the broad-line emission region as a flat disk, that is, the parameter $\theta_{open} = 0$. The disk-like BLR will be entirely on the orbital plane of the central blackhole, its inclination $i = \theta_{inc}$. In our model a disk-like BLR structure requires no angular weight, the addition of flux contributions all come from one plane. Such structures must be highly constrained in order to yield the expected broad and single-peaked BLR profile. Consider, for example, a disk-oriented face-on. The radial velocity in this case is 0 and all of the flux will be concentrated at 0 km/s, removing any broadness (the "broadness" can still exist given the convolution with the turbulent velocity profile). Hence the "disk" must be at least slightly inclined. However, the inclination must also be constrained to satisfy the requirements of the Unification Model, that the inclination must not be too high. The results are plotted in **Fig. 9**.

It is clear from **Fig. 9** that the profiles do not match the expected profiles (that is, broad and single-peaked) even at low inclinations. Typical broad-lines are relatively "gaussian" like, unimodal centered at 0 km/s and broad. While these spectra show the broadness, decreasing as a_{in}, a_{out} increases, it is certainly not unimodal and gaussian. The spectra show two symmetric peaks about 0 km/s, within 2000 km/s of separation. The peaks themselves are not symmetric about their center, distinguishing them from the profiles of two symmetric profiles generated from a binary system (more discussion see **Section 3.3**). As the outer edge of the "broad-line disk" is increased, the "dip" at 0 km/s demonstrate less and less contrast relative to the two peaks (the $a_{out} = 75\ ltdy$ line). It is expected that as this increases further the single-peak structure can be recovered.

However, such strict requirements means that it would be very difficult for a broad-line structure to form from a disk-like BLR. Moreover, as the inclination of the blackhole is increased it would allow the "two-peak" structure to become more apparent, hence suggesting that a disk-like model for the BLR is not a likely, physical model of the actual BLR. These "double-peak" structures are typical of accretion disk emission, being "disk-like" and extremely compact, allowing more broadness to the profile, many times than the typical broad-line. Such emission

mechanism will be generated with our model and described in **Section 3.2**.

Fig. 9. Results plotted for a disk-like BLR at 15° inclination. The top panel fixes $a_{in} = 20ltdy$ and varies a_{out}, while the bottom panel fixes $a_{out} = 20ltdy$ and varies a_{in}. The other parameters are: $e = 0, \omega = 0, \gamma = 0, M = 10^8 M_{sun}$ and $v_{turb} = 500km/s$.

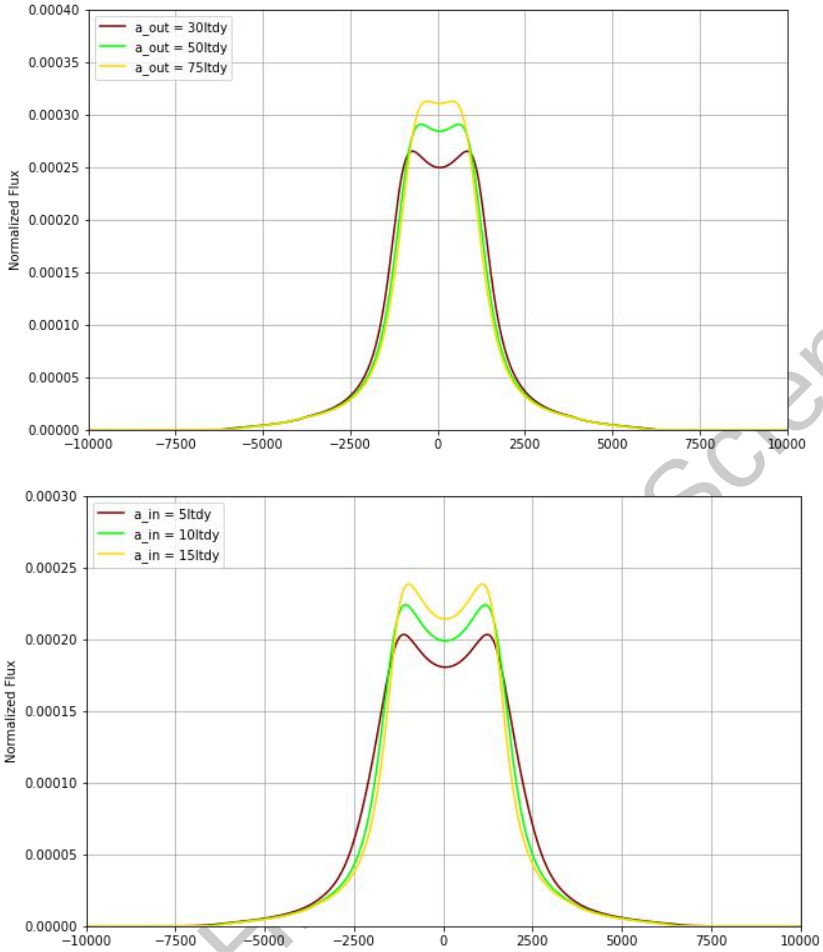

The failure for a disk-like emission region of broad-lines suggests that more parameters must be taken into consideration. In particular this requires θ_{open} to take on a value larger than 0. The added flux contributions from other orbits at different inclination fills in the dip at 0 km/s, allowing the profile to recover its gaussian-like shape.

3.1.2 Sphere-Like BLR

Spherical BLR models the line-emitting region as a "sphere", more accurately a shell, whose inner and outer semi-major axis is determined by the model parameters a_{in}, a_{out}. When placed at low-inclination blackholes, the added weight to the face-on oriented BLR orbits (by the cosine factor) will result in the profile being sharper than that of a flat-disk model. As before, we normalize the emission line curves by setting the area of the space under the profile equal to one; fitting observed spectra requires scaling by a constant.

Typical broadline profiles follow a quasi-gaussian shape, with rounded peaks and large width (up to 10,000 km/s). In our model we first verify that the spherical assumption is a valid model in describing the BLR by observing the generated flux profile.

The profile is generated from two components: One that directly comes addition of Keplerian orbits insider the BLR (the "raw" profile), and one that describes the turbulent velocity. Their respective shapes are plotted below:

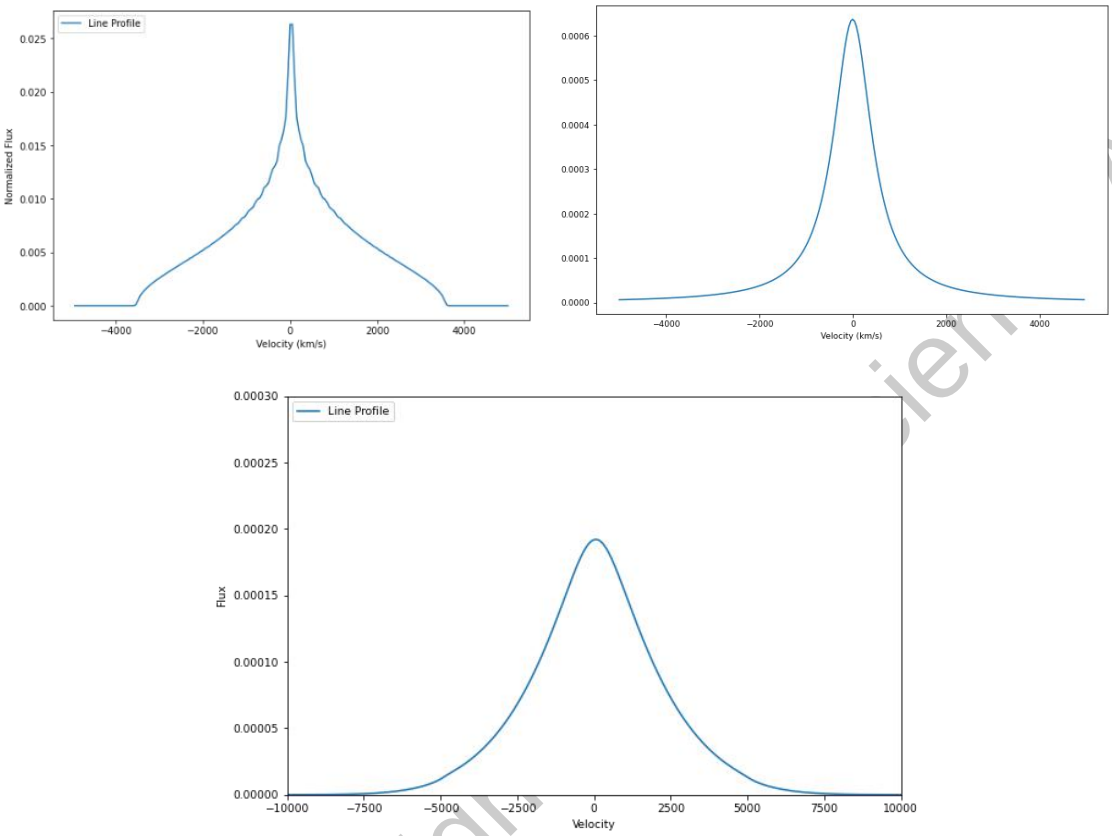

Fig. 10 Left: "raw profile" directly generated from repeatedly summing flux contributions from different orbits of the BLR. Right: Turbulence velocity profile described by a Lorentz profile. Bottom: Combined fluxes under convolution.

The center part of the "raw" profile in **Fig. 10** acts as a quasi-delta function and preserves features of the Lorentz profile under convolution. The broad width of the raw profile then adds to the final width of the profile under convolution. The resulting profile is the bottom panel of **Fig. 10**. This feature would be characteristic of a broad line profile. Note that the profiles in **Fig. 4** contains a "sharp peak", these results from the redshift from velocity space to wavelength. This shift changes the axis accordingly and produces the seemingly "sharp" peak in observed spectra.

The next step is to gauge the appropriate values of the parameters which describe the structure of the BLR, namely $a_{in}, a_{out}, \theta_{open}, e, \omega, \gamma, \beta$ and v_{turb} (see **Table. 1**). In a spherical model, θ_{open} is set to be 90°. To determine the weight parameters β and γ, We select a typical blackhole mass of $M_B = 10^8 M_S$, and define the line-emitting region to be within 20 light-days to 50 light-days. It is intrinsically clear that the parameters e and ω affect only the shape of a particular BLR orbit and hence determine the shape of the profile. To constrain our variables, we set $e = 0$, that is, a perfectly symmetric BLR, and take ω to be 15° (note that any particular value of ω will yield the same result for a circular orbit).

From the unification model (**Section 1**) Broad-line spectra appears when a blackhole is at a face-on orientation. For this reason, we set the inclination of the blackhole, θ_{inc}, to be at 15°, a relatively low inclination. Finally, effects from the turbulent velocity must be considered, and we take the value of v_{turb} to be at 500 km/s.

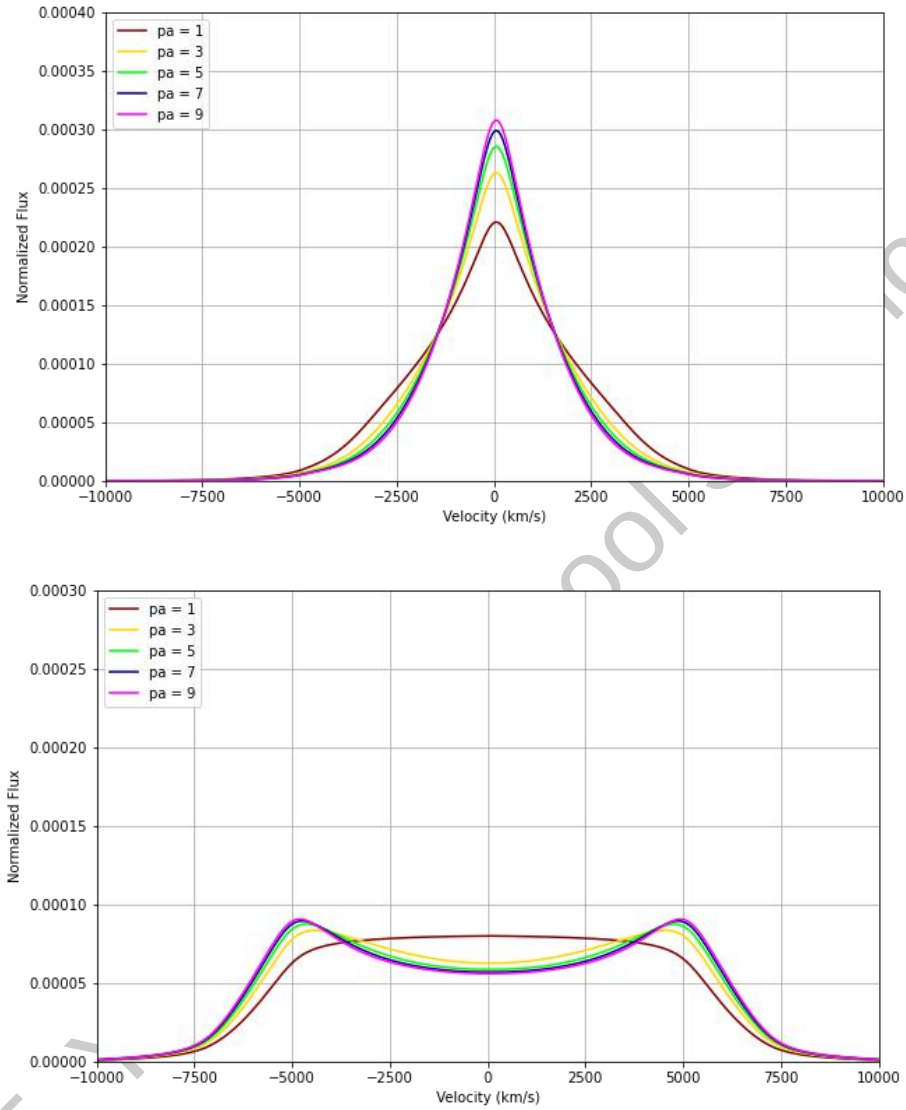

Fig. 11 Top: variation of angular power at inclination 15°, where the broad-line feature is apparent. Bottom: Variation of angular power at a higher inclination of 90°, where the "double peak" structure arises, thought to be the signature of accretion disk emission. "pa" denotes power of angular direction.

As the top panel of **Fig. 11** demonstrates, at a lower inclination, the effect of increasing the angular power constrains the FWHM (full width at half maximum), that is, with increasing angular power the profile becomes narrower and sharper. As with increasing angular power, more relative weight is added to the face-on orientation, it is expected that the flux from lower inclined orbits will contribute more to the final profile.

In addition, we note that the gaussian shape characteristic of most BLR profiles are apparent

in the model for relatively high angular power. This suggests a higher angular weight should be assigned, i.e., $\beta > 3$. The need for a relatively high angular weight calls for an enhanced influence of orbital inclination relative to the blackhole on the final broad-line profile. It is likely that, due to angular momentum considerations, in falling gas towards the BLR will be captured more often along the equatorial plane and thus for a Seyfert I galaxy, a considerable amount of BLR clouds would be located on or near the equatorial plane.

Although with increasing angular power the peak became sharper, changes are negligible as power increases higher (see, for example, the blue and magenta line, corresponding to $\beta = 7$ and $\beta = 9$) compared to lower powers. This phenomenon can be explained theoretically with reference to model construction: the final profile is obtained by the convolution of the orbital flux (the "raw" profile) with turbulent velocity curve. With increasing power, the "raw" flux will be concentrated strongly at the equatorial plane, hence reassembling a delta function. Upon convolution, the final profile will be highly dependent on the shape of the turbulent velocity curve, and hence reaches a limit where increasing angular power have negligible effects on the profile. Overall, for further modelling this encourages us to choose higher powers for inclination, as 1. With increasing power, the shape resembles a true profile, and 2. There is safety in overshooting, that is, choosing too high a power will not affect the resulting profile significantly.

We have included additional profiles for an inclination of 90°, shown in the bottom panel of **Fig. 11** As expected, with increasing angular weight the profile retains the profile from "disk-like" structures. As angular power increases the edge-on component of the BLR dominates, and as a result, the line-emitting region is capable of producing accretion-disk like emission lines. The large width of those lines results from a narrow line-emitting region, the parameters chosen constrains the line-emitting region a circular shell between 10 and 20 light-days, where the radial velocity difference is large.

Similarly, radial weight can be described as a power law with index γ. In order to isolate the effects of radial weight we assign a low weight to the angular power, i.e., $\beta = 0$, so that the orbits are distributed uniformly in space with equal emission capabilities. The resulting flux variation is shown in **Fig. 12**.

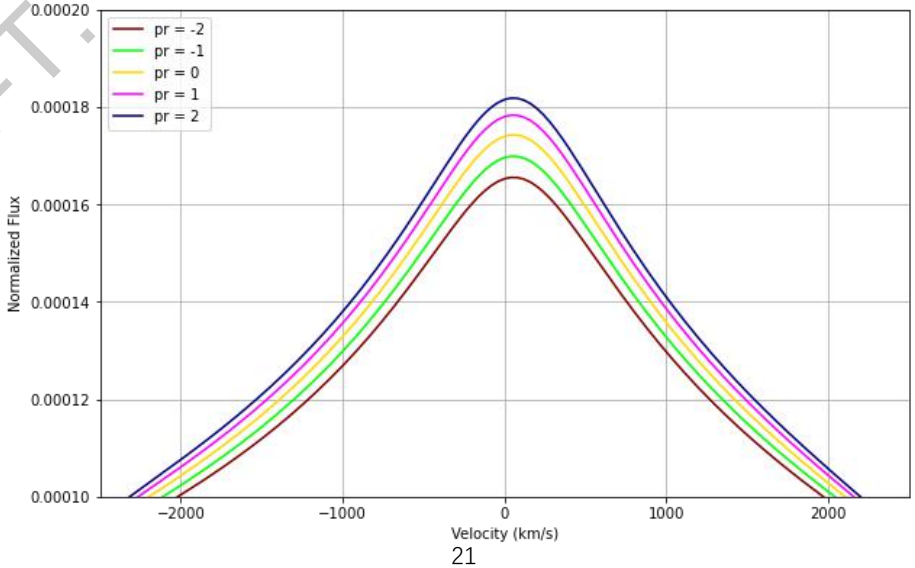

Fig. 12 Varying the radial emission capability. Image is blown up to locate small differences in peak height. Slight deviation from symmetric shape results from the "eccentricity", the eccentric factor, to be 0.3.

Fig. 12 suggests that although physically important, the effect of radial power is considerably less than that of angular weight. With each unit rise in the radial power, the peak rises by approximately 0.000005 normalized flux units, about 10 times smaller than the sharp changes due to angular variation. The relatively "parallel" profile lines also suggest only a small change in profile shape due to the change in radial power. This contrasts with the high dependence of shape on *angular power*, for example the red and yellow lines ($\beta = 1, \beta = 3$) in both plots of **Fig. 11**. With higher radial power indices, for example $\gamma = 10$ the difference may become apparent, but such a high index is physically unplausible and hence we can conclude that the constrains on the parameter γ is relatively free. This lack of dependence on radial emission power is explained by the relatively major flux contributions from face-on oriented orbits, whose flux would concentrate at ~0 km/s. Decreasing radial emission capabilities places greater contribution for the innermost regions of the BLR, whose contribution lies at higher radial velocities (i.e., >2000 km/s). This has the effect of *reducing* the sharpness of the profile peak. This relatively low affect is unable to account for the larger contribution from face-on orbits. Hence, for onward simulation we set $\gamma = 0$, that is, radial emission capability is constant throughout.

The eccentric parameters e, ω determine the asymmetricity of the profile. Profiles with $e = 0$ are perfectly symmetric and centered at 0 km/s as the ones shown in **Fig. 11**. For profiles with some degree of eccentricity, such as those shown in **Fig. 12**, The "red" (positive radial velocity) slope and the "blue" (negative radial velocity) slope are inclined differently according to the parameter ω. In particular for the case of **Fig. 12**, $\omega = 0$ and the peak is slightly red-shifted, that is, not centered a 0 km/s.

When constructing models to differentiate the variation of eccentricity, the inclination must be chosen to be relatively high. This is because as the angular power must be chosen to be high, flux contributions will be concentrated at the face-on oriented orbits, whose contributions lie at 0 km/s. Under these conditions the effect of eccentricity cannot be determined, and hence we chose the inclination, θ_{inc}, to be 30°, allowing the formation of BLR at a higher inclination. ω is chosen to be 0, and all other parameters are fixed as before. The resulting profiles are drawn in **Fig. 13**.

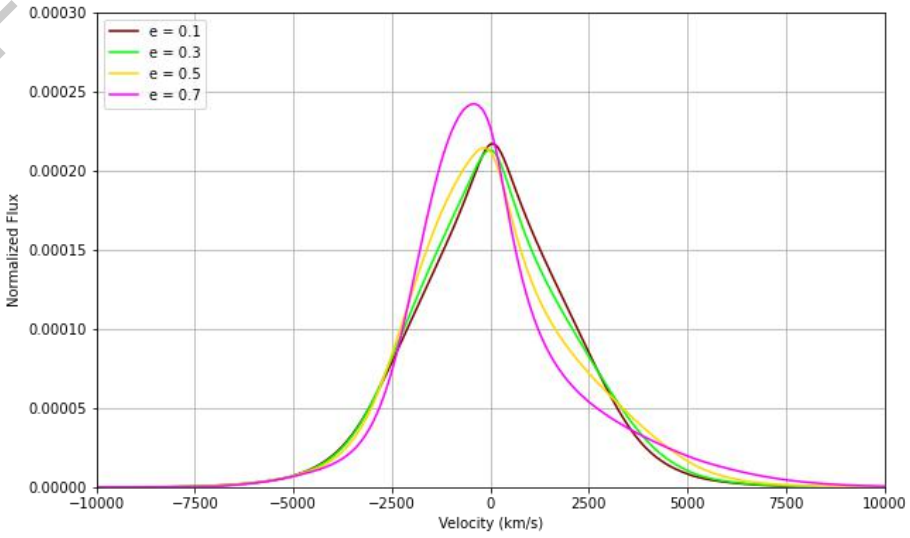

Fig. 13 Profiles of eccentric orbits. Note this particular type of variation is specific to a chosen ω.

Eccentric profiles demonstrate a horizontal and vertical deformation, attributed to the now non-uniform velocity along the orbit. For $\omega = 0$, with increasing eccentricity, the profile shifts to the left with distortion to the red and blue slopes. In particular, the high radial velocity tail of the profile is redshifted to 10,000 km/s for an eccentricity of 0.7, compared to the ~7500 km/s for eccentricities of 0.1 and 0.3. For higher eccentricities the lost of symmetricity is apparent; although for lower eccentricities the difference is negligible, larger eccentricities show a rapid distortion and increase in peak sharpness. The effect of eccentricity can roughly be described as $\frac{1}{\sqrt{1-e^2}}$. For eccentricities smaller than 0.5 the effect is smaller than approximately ~1.15. Physically it is rare for highly eccentric orbits to be observed; such orbits are prone to disruptions and may easily shift to an escape orbit or a lower eccentric one. Hence although higher eccentric orbits are plausible for our model, physically accepted profile would be ones of low eccentricity, roughly speaking <0.5, whose peaks would be centered at 0 km/s as shown in **Fig. 13**.

The symmetrical and asymmetrical properties of the line profile are also determined by the argument of pericenter, ω. For single orbits the argument of pericenter describes the position of the pericenter (closet approach to center mass), with 0 being horizontal to observer. While for circular orbits any argument of pericenter will yield the same result, eccentric orbits yield different flux profiles due to the dependence on ω in the radial velocity equation: $v_r = K(\cos(\omega + \nu) + e\sin\omega)$. Thus, we expect a different degree of eccentricity for different values of ω.

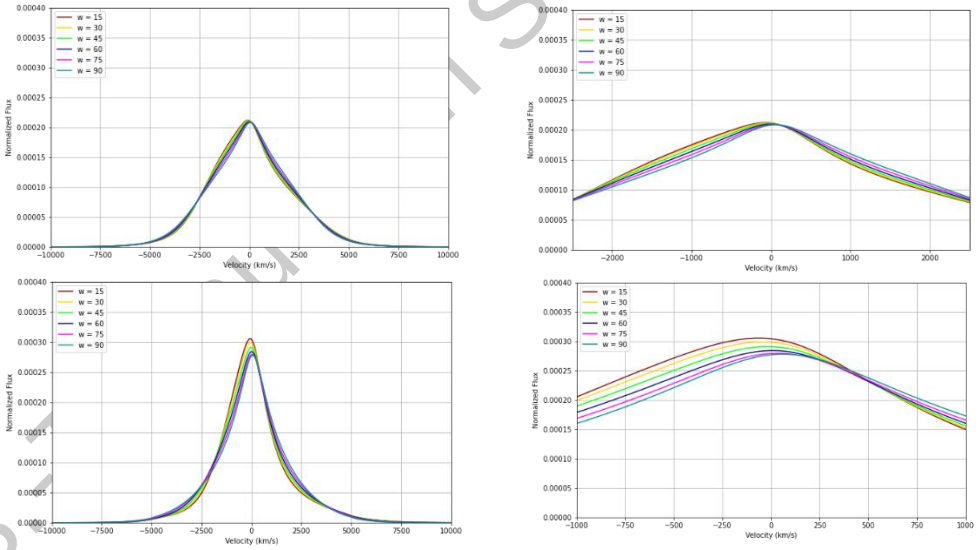

Fig. 14 top-left: Varying ω for inclination of 30°. Subtle differences are shown in top-right, blown-up image. bottom-left: Varying ω for inclination 15°, and its blown-up image bottom-right. Note that ω can take values higher than 90°, but due the geometry nature of the BLR, higher values of ω will yield the same pattern of variation but shifted to the right. The eccentricity chosen is 0.4.

The variation of ω is related to the direction of the now asymmetrical broad-line region. Time-dependent rotations due to the blockhole's self-motion may result in a time-dependent variation of ω and hence in the profile. In particular it would be necessary to distinguish natural variation of the BLR itself to that of binary blackholes, whose variation pattern would be predicted

by Kepler's Laws.

The variation of ω, unlike that of eccentricity, gives negligible change in the shape of the profile, but rather a systematic "velocity shift", in which the peak magnitude is decreased and shifted to the right ("red-shifted"). The magnitude of such variations are considerably smaller than that expected from Keplerian variation, as shown from **Fig. 14** a) and c). The enlarged image shows a typical variation of~25 km/s with each 15 degree increase in ω for inclination of 15° and even less for higher inclinations. (**Fig. 14** b) and d)). Such small variations are usually unresolvable on spectrographs (the SDSS surveys have a resolution of ~50 km/s) and easily mixed with other, natural variations. Keplerian variations are of the order ~1000 km/s and hence easily distinguishable from those of ω. In conclusion, for spherically-modelled BLR, eccentricity affects the shape of a profile significantly for larger eccentricity, although the effect is also noticeable for smaller eccentricities. Variation of the parameter ω yields lesser results on the profile with the profile lines grouped closely together.

The parameters a_{in}, a_{out} define the span of the broad-line region. An important concept is that the spread in radial velocity increases as the semi-major axis of each orbit decreases. This is due to the expression for the radial velocity semi-amplitude:

$$K = \frac{2\pi}{P}\frac{a\sin i}{\sqrt{1-e^2}}$$

The period P contains $\sim a^{1.5}$ dependence and hence overall K scales as the square root inverse of the semi-major axis, $\sim a^{-0.5}$. Thus, with decreasing a_{in} the result would be predicted to be a broadening of the profile, and vice versa. Similarly, decreasing a_{out} results also in a broadening of the profile, as the flux contribution at low radial velocities are lowered, and normalization results in the broadening of the profile. We shall first observe the variation of the parameter a_{out} as it is defined over a larger range (refer to **Table. 1**), from 20 light-days to 100 light-days. The parameter a_{in} is constrained to a narrow range (10 to 20 light-days), so that its effect on the profile will not be distinguishable (see **Fig. 15**).

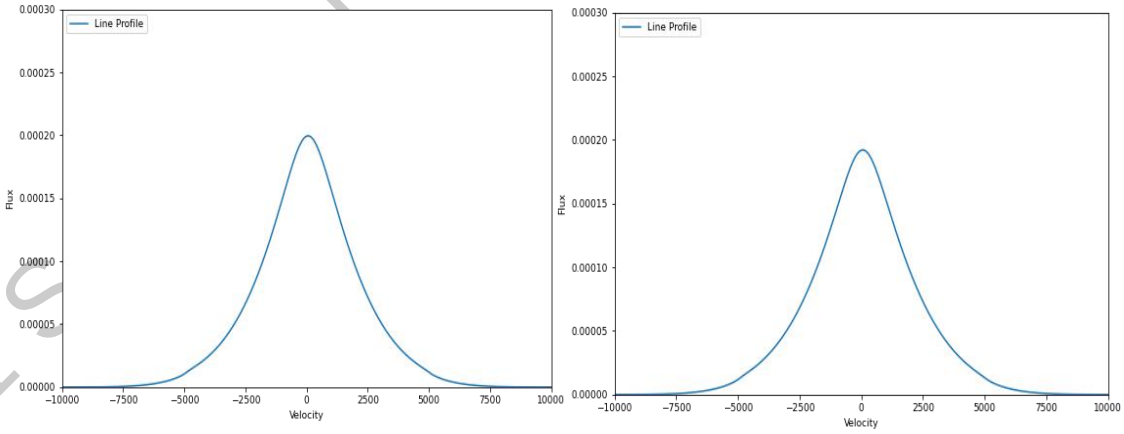

Fig. 15 Left: Profile for spherical BLR of 10 to 20 light-days. Right: Profile for spherical BLR of 15 to 20 light-days. Note the lack of distinguishable variational features. All other parameters were kept the same: $\theta_{inc} = 0°, \theta_{open} = 90°, e = 0, \omega = 0, \beta = 7, \gamma = 0,$, $M = 10^8 M_{sun}$ and $v_{turb} = 1000\frac{km}{s}$.

To allow variation differences to be distinguishable we plot the profiles at 20 light-days steps

from 20 light-days to 100-light-days. The results are plotted in **Fig. 16**. Note that different plots were created for different inclinations (0 and 30°).

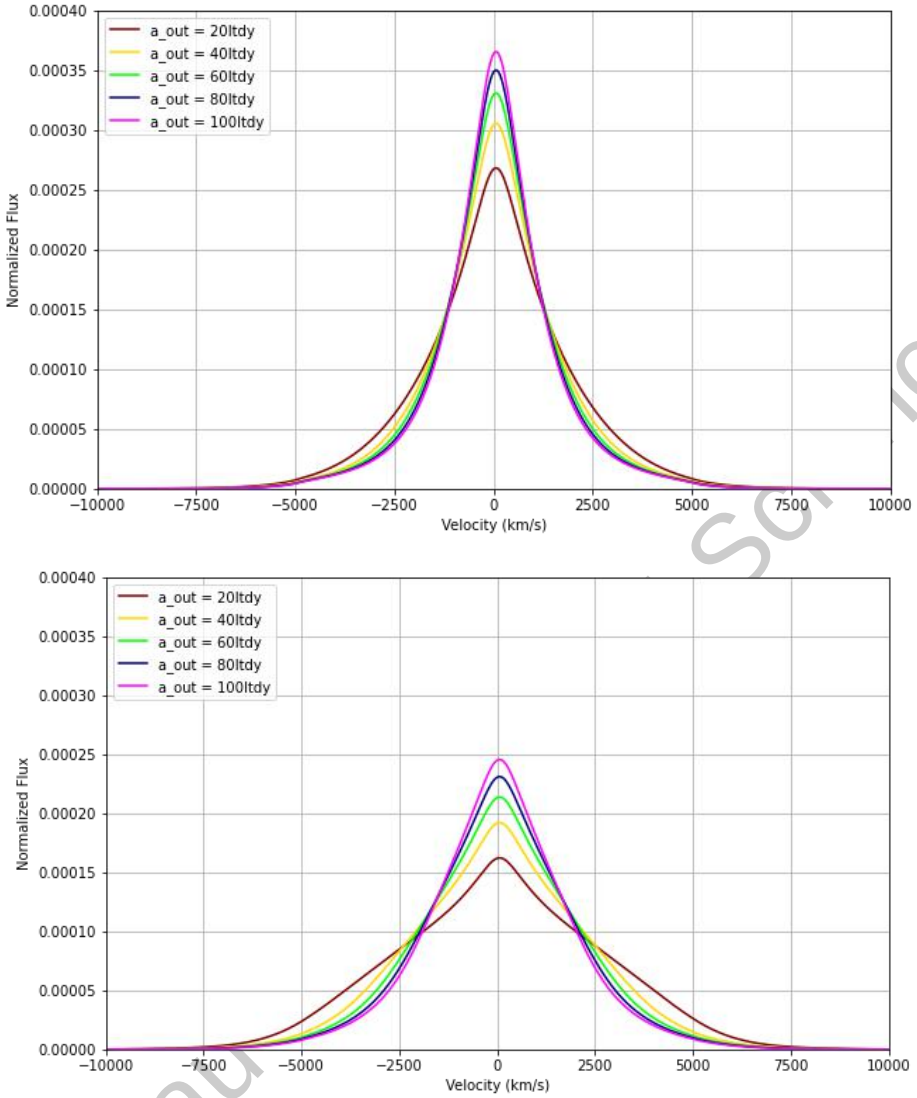

Fig. 16 Top: Profiles for 0° inclination. Bottom: profiles for 30° inclination. Note the differences in profile for different inclinations which will be discussed later. The broadening of the profile is coupled with the lowering of the profile peak, this is a result of normalization: since more flux is coming from higher radial velocities, the relative flux of the lower radial velocities must be lowered.

Fig. 16 Demonstrates the expected results from varying the parameter a_{out}. With increasing a_{out} the profile loses its broadness, as expected: relatively more flux is coming from outer parts of the BLR where the radial velocity is low. Notice also that for lower inclinations (Top of **Fig. 16**) the profile's shape is not changed significantly, only its width is reduced. Similar to variation of angular power, this effect is somewhat reduced for higher a_{out}, for example compare the difference from varying a_{out} from 20 to 40 light-days and from 80 to 100 light-days. This can be explained by realizing that higher a_{out} gives more relative weight to outer regions of the BLR where the radial velocity is low. Under convolution the turbulent velocity profile dominates due to the appearance of the "raw" profile to be a delta function (consider **Fig. 10**).

At higher inclinations the variation becomes more extreme. At an inclination of 30°, smaller a_{out} differs greatly from higher values. At $a_{out} = 20$ light-days, the profile loses its "gaussian" shape and instead withheld a triangular shape. The FWHM (full width at half maximum) is also seen to be larger than most profiles, going well past 5000 km/s. As a_{out} is increased, however, the "gaussian" shape is recovered as of the case for lower inclinations, although it is slightly broader. Overall, it can be seen that for higher inclined blackholes, in order to generate the correct profile a higher value of a_{out} must be chosen to make up for the flux lost due to inclination.

It is also apparent that the role of inclination is to play a major role in determining the differences in profiles. Note, for example, the completely different profiles at different inclinations in **Fig. 11**. The effect of inclination would serve as a final test for the validity of our model, and the results for the profiles plotted at different inclinations are included below. Note that in reality only the profiles that appear at low inclinations can be seen due the Unification model. However, it would be of interest to demonstrate how inclination can dramatically affect the appearances of the profiles.

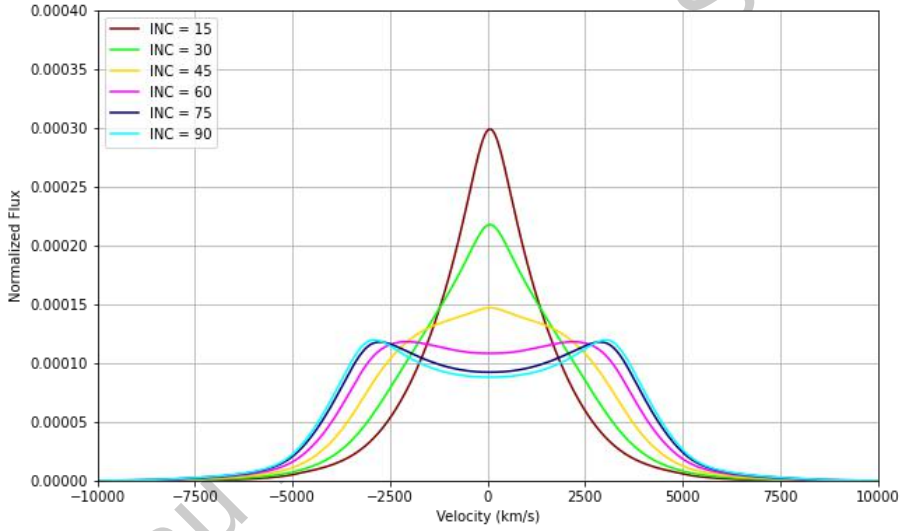

Fig. 17 Variation of inclination for a spherical BLR. Note the dramatic change from a gaussian-like profile to that of a double peak structure. Parameters are chosen such that the profile is symmetric (e = 0), $a_{out} = 50\ ltdy$ and $a_{in} = 20 ltdy$.

The effect of inclination to the profile is seen to be dramatic in **Fig. 17**. With increasing inclination, the broad-line feature of the profile slowly reduces to that of a profile from a "disk" structure. The two peaks in the profile reach a limiting position inclined at 90°, its peaks well to the left of -2500 km/s and to the right of +2500 km/s. In the region where the broad-line structure is apparent (single-peaked) the change is quite dramatic. Changing the inclination from 15° to 45° results in nearly a 50% decrease in the profile peak and significant broadening. This suggests a heavy reliance of the profile on the inclination angle θ_{inc}. This is partially due to the need to give a relatively high angular power β. In effect, this also explains the wide variety of broad-line features among single AGNs as those resulting from different inclinations. The results of our model suggests that only low-inclined AGNs can yield the expected profile structure, the profiles of higher inclination are not seen because of the "gas torus" blocking emission lines from higher

inclined AGNs, according to the Unification Model.

However, it is known that the "double-peak" structure at high inclination has also been observed superimposed a broad or thin emission line. This suggests that it would also be possible for such structures to form at lower inclinations, particularly for where the emission region is small—less than 5 light-days from the central blackhole, where the accretion disk is thought to be at. This will be discussed in section **3.2**.

3.1.3 Ring-Like BLR

In past discussions the modelling parameter θ_{open} was always taken to be 90°, or a spherical model. However different conformations of the BLR also exist, where the BLR clouds no longer cover all of space but spans a "ring" structure, an intermediate between the "disk" model and "sphere" model.

In this section we vary the parameter θ_{open} to identify variation features of the profile. For low-inclined orbits, the reduction in the opening angle results in less flux contribution from orbits of the edge-on orientation, so that relatively more flux is coming from the face-on orientation. Such changes to the parameter will result in the profile becoming sharper (more flux at ~0 km/s radial velocity).

As before, in order to isolate the effect of θ_{open}, we fix the other parameters: the BLR ranges from 20 to 50 light-days with an inclination of 15°. The "shape" parameters e and ω are chosen to be 0 so that the profile is symmetric. Angular weight and radial weight are 7 and 0, respectively. Finally, a blackhole mass of $10^8 M_{sun}$ and a turbulent velocity of $v_{turb} = 500 km/s$ is selected. The resulting profile is plotted in **Fig. 18**.

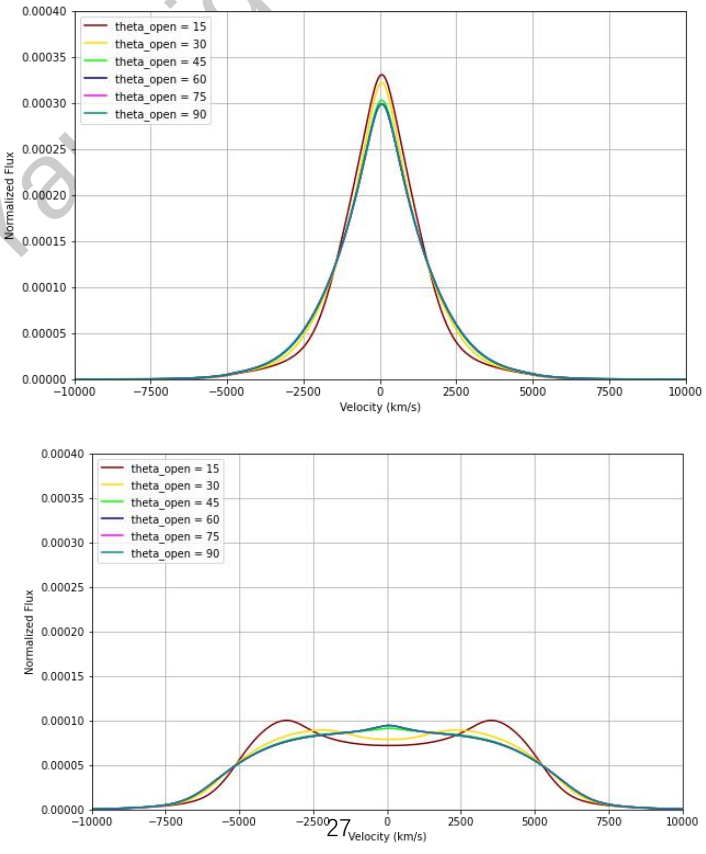

Fig. 18 Top: Profiles plotted for a low inclination (15°). Bottom: Profiles plotted at a higher inclination of 45°. Note that the profiles plotted at 45 degees inclined has a smaller BLR than that of **Fig. 17**, so that the "double-peak" structure also appears.

Two plots were created to observe differences of the profiles at different inclinations. The profiles that have an inclination of 45 degree were defined to have $a_{in} = 10\ ltdy$ and $a_{out} = 15\ ltdy$. Note that at opening angles of 15 and 30° the "double" peak structure appears, whereas in **Fig. 17** at 45° the profile is still very much a "single" peak (the BLR in **Fig. 17** ranges from 20 to 50 light-days and has 90° opening angle). This suggests that it may be possible to form "double peak" structures to form at low inclinations given that the emitting region is disk-like and its semi-major axis small (an accretion disk).

The variation at higher inclination is expected as with smaller opening angle, more flux is concentrated to one highly inclined "disk" and thus show the two-peak structure present in accretion disks. Finally, as the opening angle increases, we see the clear trend of the double-peak reducing to a single-peak, though clearly not the expected profile for a broad emission line. This trend reaches a critical value after an opening angle of 45°, where the lines are grouped closely together. For higher inclinations and at high opening angles, the variation of the profile due to changes in the opening angle is negligible.

At lower inclinations the profiles maintain the general "gaussian" shape, with a single peak and not unlike most BLR profiles. The variation of opening angle in this case introduces only little change in the profile, primarily in the peak height without significant broadening. The maximum difference between the maxima of the profiles is less than 0.00005 units (approximately 0.00003), comparatively less than 10 % of the profile maximum.

3.2 Double-peaked Single AGN emitter

Previous discussions concluded that at low inclined structures, the model generate the typical broad line structure. However, when the line emitting region is disk-like as described in the previous section it is possible that a "two-peak" structure appears, even at lower inclinations of 15° in **Fig. 9**. However, such profiles are much too narrow, with width equivalent to that of a broad-line width. Two-peaked structures observed in AGN generally are extremely broad, many times broader even than broad-lines. If such lines are to be Doppler-broadened, they are of up to ~10,000 km/s. Usually such broad components are observed in low-luminosity AGNs (LLAGN), for example in **Fig. 18**, but Storchi-Bergmann et al. (2017) suggests that such structures may also appear in Seyfert Is, or low-inclined AGNs. The inner most parts of the BLR may constitute part of the accretion disk and holds similar emission mechanisms to the rest of the BLR. In such regions close to the central blackhole the line width can reach up to 10,000 km/s under the strong gravity, while the disk-like structure that differentiates the accretion disk allows for the double-peak structure.

When observed in LLAGN where the broad-lines are rarely present, the emission profile is easily identifiable, sometimes with a set of thin-emission line superimposed on top (see **Fig. 19**). However, if the range of the emitting region (that is, a_{in}, a_{out}) is chosen to be small enough, the

profile in **Fig. 9** can be broadened to ~10,000 km/s at lower inclinations. Such spectra will consist of a broad-emission line resulting from the exterior BLR and a two-peak profile from inner parts and the outer edges of an accretion disk, superimposed on another. However, even in such conditions it would be rare to observe distinguishable structures of both the BLR and the double-peaked emitter. More likely observed are the type of AGN shown in **Fig. 19**, with no or rather weak component of the broad-line.

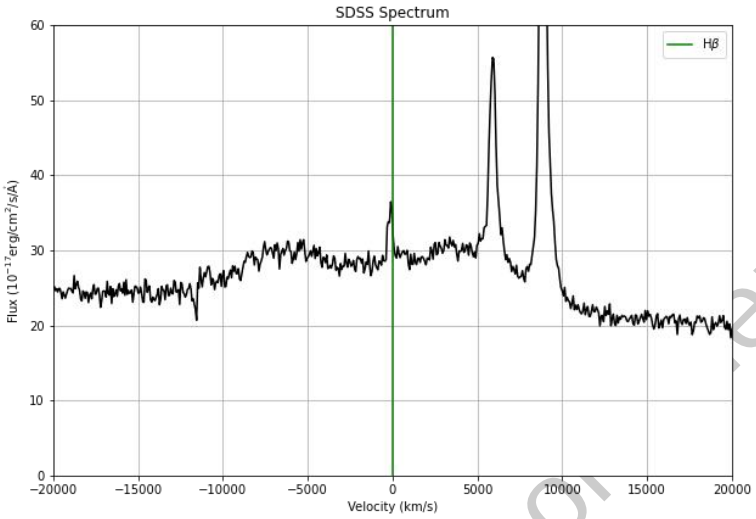

Fig. 19 Emission spectra of the $H\beta$ region of the AGN J123807.77+532556.0 (in SDSS database). Note the appearance of the double-peak centered at 0 km/s. The strong lines between 5000 km/s and 10000 km/s are the O[III] thin lines.

Stronger broadlines are likely to be able to "absorb" the weaker double-peaked emitter and are observed only as a slightly broader emission line. Hence the more intriguing cases are the profiles with very strong double-peak structures, as in **Fig. 19**.

In **Fig. 20** we attempt to fit the spectra of J123807.77+532556.0 with model predictions. The continuum emission is subtracted by best-fitting a 7th degree polynomial for the line-free region, by removing the strong $H\beta$ and $H\alpha$ lines. This AGN is found to be at redshift $z = 0.3477$. The observed (redshifted) wavelengths are shifted back to the center-of-mass frame, $\lambda_0 = \frac{\lambda_{observed}}{1+z}$. This is then corrected to velocity space using the doppler shift equations. For our purposes we are interested in the strong Balmer lines $H\alpha$ and $H\beta$. The velocity space for each emission line is found by $v_\alpha = \frac{\lambda-\lambda_\alpha}{\lambda_\alpha}c$ and $v_\beta = \frac{\lambda-\lambda_\beta}{\lambda_\beta}c$.

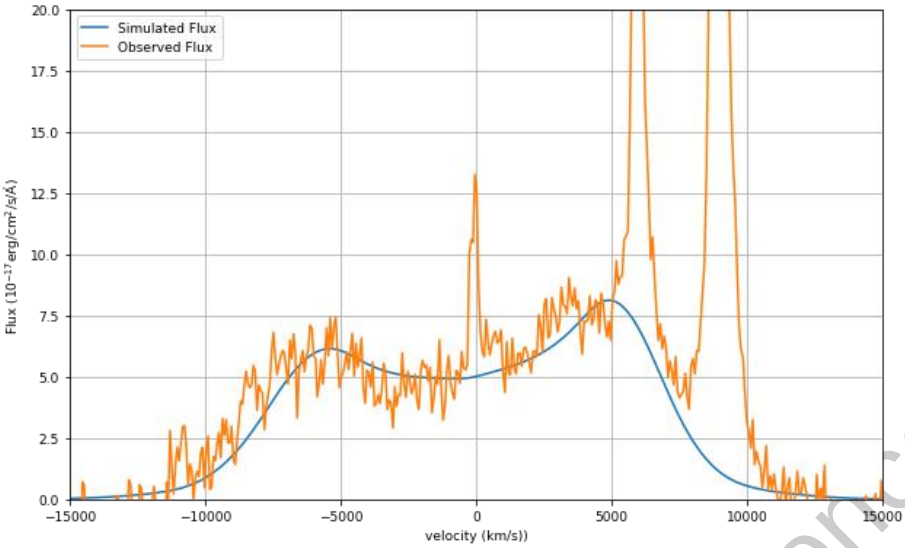

Fig. 20 Fit of the $H\beta$ region of the AGN J123807.77+532556.0. The sharp rise at 0 km/s is due to the $H\beta$ narrow-line, which is stationery in the center-of-mass frame. Deviations at 5000 km/s~10000 km/s are due to the O_{III} narrow lines.

The relative broadness of the profile suggests a highly compact emitting region; the line-emitting region is constrained to be in 1~2 light-days, at approximately 1000 gravitational radii. Even at such highly compact space, a low inclination may still result in the absence of the double-peak structure. Thus, keeping to the Unification Model, an inclination of 20° is chosen. Finally, the double-peak holds an asymmetric profile with a stronger "red" side than the "blue" side, and the center of the profile lays to the left of the narrow-line. This suggests an overall eccentricity should be included in the model. Testing found that e = 0.3 and $\omega = 150°$. The turbulent velocity is chosen to be 500 km/s.

The theoretical emission profile agrees with the observed spectra well in the $H\beta$ region. The simulated flux profile is able to account for the general shape of the observed emission line, describing two peaks approximately 10000 km/s apart, with a small dip leftwards of the center-of-mass radial velocity (0 km/s). The profile also suggests that broad, up to more than 10,000 km/s in width, profiles can be generated at relatively low inclinations (20°), explaining their appearances in some Seyfert I spectra.

It is interesting to note the lack of a superimposed broad-line structure on top of the double peak profile for most AGNs. Generally, if the broad double peak structure can be observed at lower inclinations, the likelihood of such an emission line appearing alongside a broad-line and a narrow-line is quite high. The lack of the broad component (see spectra in Storchi-Bergmann et al., (2017)) suggests that in the case of a double peak structure being observed, the broad component of the spectra must be relatively weak. This could be understood in terms of the higher ionization rate closer to the blackhole as well as the increased electron density compared to the BLR. **Fig. 21** plots the respective spectra for different strengths of the "double-peak" emission.

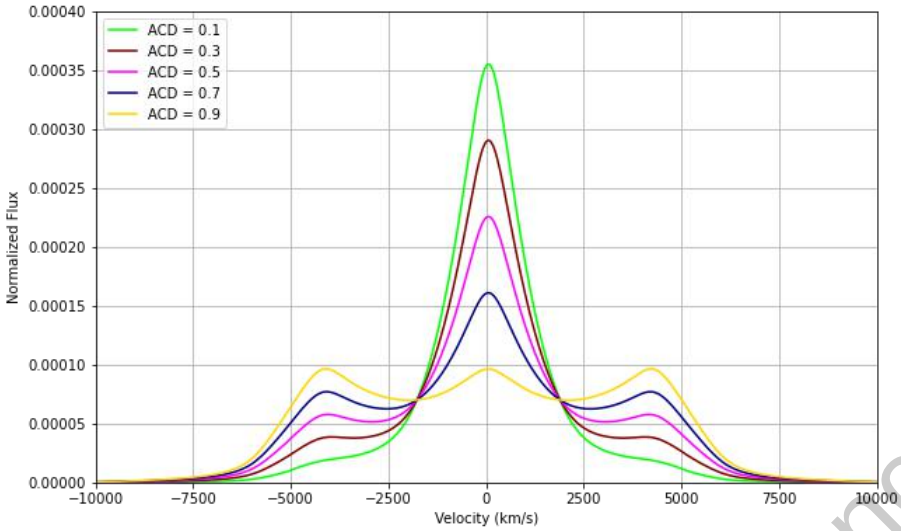

Fig. 21 Resulting spectra for different strengths of the broad-line and double-peak emission. "ACD" denotes the weight assigned to the double-peak component; the broad component is assigned weight 1- ACD.

When double-peaked structures are observed, the (theoretical) transition between the broad-line structure and the double peak structure can be seen to become sharper with increasing double-peak emission (and lower broad-line emission). At lower weights for the double-peak structure, however, the transition is less clear. In practice sufficiently high SNR (Signal-to-noise ratio) prevents these features from being observed. The result is that the "double-peaked" emission is absorbed into the stronger broad line emission, giving just a single broad peak. Only when the double-peaked component is significantly stronger than the broad-line emission, i.e., ACD>0.9, does the "double-peak" structure become apparent. In such extreme conditions the broad-line component is mostly ignored or hidden by noise, resulting in double-peaked profiles up to ~10,000 km/s in width.

3.3 Binary Black Holes Candidates Selected by Their Featured Emission Lines

In this section we explore the structure and profiles of emission lines resulting from binary AGN cores. Binary AGN cores at Keplerian separation (under the influence of gravity) have an additional set of radial velocity calculated as described in **Section 2**. The radial velocity changes with respect to time according to $v_1 = \frac{2\pi}{P}\frac{M_2}{M_1+M_2}a_* \sin i\ (\cos(\omega + \nu(t)) + e\cos\omega)$, and $v_2 = \frac{2\pi}{P}\frac{M_1}{M_1+M_2}a_* \sin i\ (\cos(\omega + \nu(t)) + e\cos\omega)$. The flux generated from each respective AGN are shifted by their respective velocities on the spectrum. The period depends on the total mass as well as the cube of the "total" semi-major axis a_*, and hence the radial velocities depend solely on the masses of the AGNs, as well as a_*. Finally, we note that the AGN cores are constantly moving on their Keplerian orbits and hence their radial velocities are shifting periodically according to the dynamical nature of the AGN orbit. This means that binary emission lines will evolve and change periodically with period equal to that of the binary AGN orbit. Such variations are, however, small, as the period ranges up to decades and even centuries, hence at any times the observation of the lines is essentially a stationery feature.

A power confirmation of the existence of binary AGNs is the evolution of the profile with time according to the Keplerian variations predicted by our model. However, as mentioned the period of orbital motion is long compared to observation time, hence identifying binary AGNs via such a method is impractical and time-consuming, requiring great lengths of observation for many targets. Hence the first step to identifying binary AGNs is to identify possible candidates. Selecting possible *candidates* based on spectra features associated with binary systems to limit the number of targets greatly improves the achievability of observing Keplerian variation of targets. Such observations would then help to *confirm* the candidates, if Keplerian variation is observed over some time, or rejected if vice-versa.

This section is then divided as follows. **3.3.1** to **3.3.3** describes spectral features associated with binary AGN systems and the fitting of the model to observed profiles, and their variability with time. In the final section we will select a range of binary AGNs candidates from some 1000 targets selected from the SDSS survey, selected from the QSO class with high S/N ratio.

3.3.1 Twin Broad Peaks with Velocity Offset

When two AGNs are at large enough radial velocities their respective broadline structures can be easily identified. Each respective broadline are not disrupted by flux contributions from the other, and in most cases the gaussian-like shape is preserved (**Fig. 22**). In order for the peaks to be isolated instead of merging into each other, the center of the profile (the "valley") must be lower than each broad-line. If the full width at half maximum (FWHM) is σ_1 and σ_2, a rough estimate would require the velocity separation of the peaks to be at least larger than $\frac{\sigma_1+\sigma_2}{2}$, for if not the central flux may exceed that of the twin peaks. This requires the velocity separation to be of the order of magnitude of the FWHM, ~5000 km/s, or smaller if narrower lines were used. Finally, in order for the two broad-line peaks to be a dominant feature, the flux contributions from each AGN must be relatively similar.

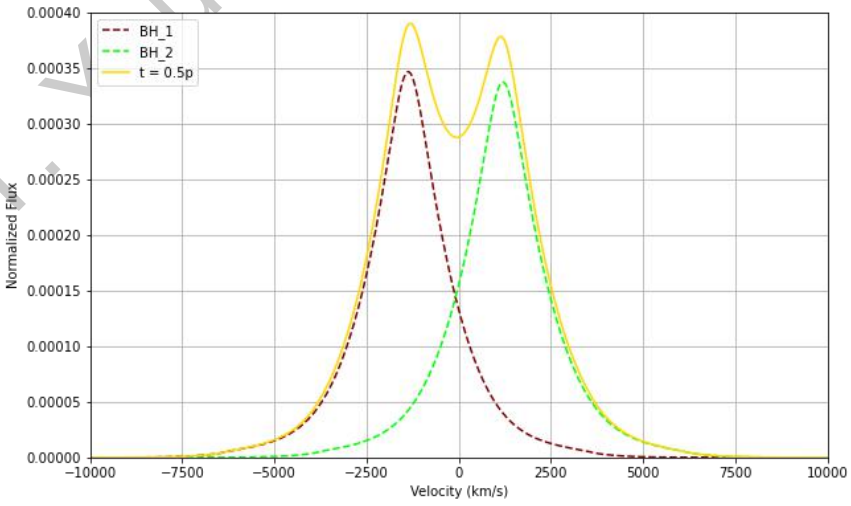

Fig. 22 A suggested model for a binary "twin-peak". The AGN masses are $10^{8.3}$ and $10^{8.4}$ solar masses, respectively, and the separation is 100 light-days for higher velocity separation.

In **Fig. 22** a suggested "twin-peaked" profile is plotted. Both broad-line regions of the two AGNs are spherical and inclined at 0°, with the clouds ranging from 20 to 50 light-days and 20 to 60 light-days. The resemblance of each "peak" to individual AGNs is also clear, when comparing the solid and the dotted lines. The outer edges of the profile closely match the broad-line profile due to small contributions from the other AGN. Between the peaks of the profile the combined flux deviates from the individual AGNs to form a "valley" centered at approximately ~0 km/s. Overall at high velocity separations it is possible for the two broad-line structures to overlap as little as possible, allowing an intuitively simple construction of two broad peaks with little difference from their original flux profile.

The different structure between such binary AGN and single AGNs allows simple selection. The "twin-peaks" are easily isolated from single peaked single AGNs, and hence makes the appearance of "twin-peaks" in all powerful candidate. There is, however, another explanation. It should however be cautioned that accretion disk spectra bear resemblance to the "twin-peak" structure (refer, for example, to **Fig. 19** and **20**) as double peaked emitters. Such emission spectra differ from twin-peaked spectra in their extreme width, ranging up to more than 10,000 km/s due to the close proximity to the blackhole of the accretion disk. In order for binary AGNs to produce separations of the same order the distance must be very close in a small scale of accretion disks and hence highly unlikely to be a binary candidate if no significant periodic optical variation.

The time-variation of twin-peaked profiles are expected to be relatively fast and easy to observe. The requirement for high velocity separation of the broad-line peaks leads to close binaries (small a_*) or high AGN masses. These requirements on the parameter ensures a comparatively smaller period P, given by $P^2 = \frac{4\pi^2 a_*^3}{G(M_1+M_2)}$. Calculation with the previous parameters ($a_* = 100\ ltdy, M_1 = 10^{8.3} M_{sun}, M_2 = 10^{8.4} M_{sun}$) gives a period of roughly 39,196 days, or 107 years.

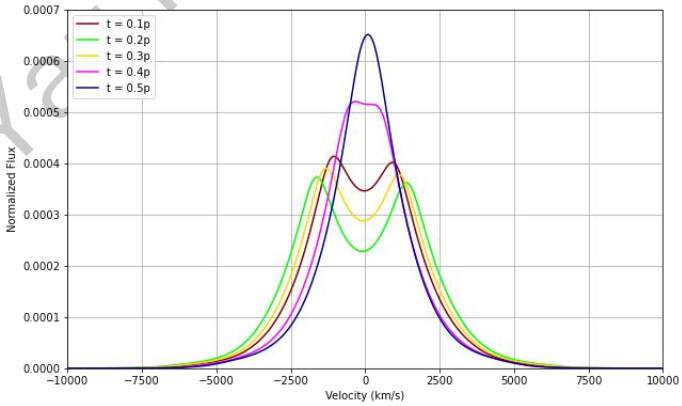

Fig. 23 Variation of the profile with time. The lines are plotted with increments of 0.1P, and plotted until 0.5P, where the profile begins to repeat the pattern.

The expected result for the periodic variation of the profile is plotted in **Fig. 23**. A key variation feature is the "merging" of the binary peaks, which is important to observe. Positions where the radial velocity is small will result in the interference of the two broad-line components produce a narrower "twin-peak". Eventually when the AGNs line up to the observer's line of sight the profiles merge into one and bears to distinct difference to that of a single AGN ($t = 0.5P$). The

observation of the periodic appearance and disappearance of the "twin-peak" feature takes place on a timescale of decades ($0.1P$~$10\ yr$).

The wide range of magnitude change for the "twin-peaked" profile can also serve as an identification of a binary candidate, where the luminosity can be seen to be almost doubled from $t = 0.3P$ to $t = 0.5P$. Such a significant change over just around two decades can almost be regarded as almost instantaneously. If a binary candidate was identified based on its twin peaks, an observer can expect to see significant amounts of magnitude variation in times on the order of decades, hence confirming the existence of a binary AGN.

Such features, despite their unique characteristics and large time-variations, are rarely observed due to strict requirement of rather close binaries, or large differences in mass. We instead attempt to test our model on one of the most well-known "twin-peaked" binary candidate to date: the AGN(s) J1536+0441 (see **Section 1**). Boroson et al. suggested a velocity separation of ~3500 km/s and AGN masses of $10^{7.3}$ and $10^{8.9}$ solar masses should be appropriate for such a "twin-peak" structure. Our goal is then greatly simplified with the orbital parameters of the two AGNs determined, and fitting is done by finding appropriate values for the BLR of both AGNs.

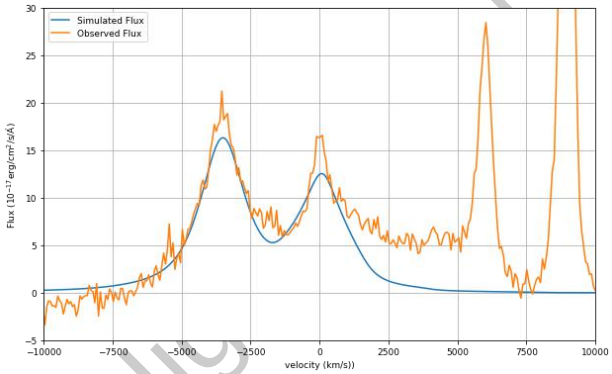

Fig. 24 Fitting of the "twin-peak" broad-line J1536+0441.

The objective of fitting the profile is to describe the "twin-peak" structure via our model. In **Fig. 24** the observed and model flux is plotted (after subtracting continuum emission). The parameters are shown in **Table 2**.

Parameter	AGN1	AGN2
$\mathbf{a_{in}}$	20 ltdy	40 ltdy
$\mathbf{a_{out}}$	50 ltdy	50 ltdy
$\boldsymbol{\theta_{inc}}$	0	0
$\boldsymbol{\theta_{open}}$	90	10
$\mathbf{e}$	0	0
$\boldsymbol{\omega}$	130	0
$\boldsymbol{\gamma}$	0	0
$\boldsymbol{\beta}$	7	7
$\mathbf{v_{turb}}$	500 km/s	300 km/s
$\mathbf{M_B}$	$10^{7.3}M_{sun}$	$10^{8.9}M_{sun}$

Table 2 Parameters for the "twin-peaked" binary candidate J1536+0441

The masses of the AGNs in the binary system can be seen to be of a great difference. Peaks with similar masses have radial velocities that are symmetric about v = 0 km/s, for example **Fig.**

23. The profile identified by Boroson et al. suggests that one AGN is essentially stationery at 0 km/s, and the other approximately blue-shifted by 3500 km/s, explaining the large difference in mass ($M_1 v_1 = M_2 v_2$). The peaks from the profile however are seen to be quite similar, and hence parameters for AGN2 must be chosen so its profile is significantly narrowed. The turbulence velocity is hence reduced to 300 km/s and the shape of the BLR chosen to be "disk-like". The model describes the profile quite well, generating the "twin-peak" structure required, roughly following the shape of the two peaks. This structure is repeated in all of the Balmer lines on the SDSS spectrum, and hence strongly indicate that the AGN system J1536+0441 is a binary candidate.

Twin-peaked binary systems, as discussed previously, have large variations in magnitude over short periods of time. At such high velocity separation, the time period is even smaller. Confirmation of this candidate would require large variations both in the profile structure (merging of the peaks) and magnitude in a short time.

3.3.2 Single Broad Peak with Systematic Redshift

Binary AGN are rarely located on the celestial sphere, and it is even rarer to find close AGNs interacting to produce "twin-peaked" profiles. The generation of "Twin-peaked" profiles requires not only large velocity separations, but also that both blackholes must be active. This is not always the case, considering the short duty cycle for activate blackholes and AGNs can have a high degree of variability in their luminosity. In such a scenario where the velocity separation is not as large, and one of the AGN is weaker than the other, we obtain a "Weak-component" Twin-peaked spectra. In such profiles one broad-line is partially absorbed into the other, generating an altogether different profile than single AGNs and "twin-peaked" structures.

Cases where the magnitude difference is not extreme retain some of the properties of "twin-peaked" structures, for example in **Fig. 25**

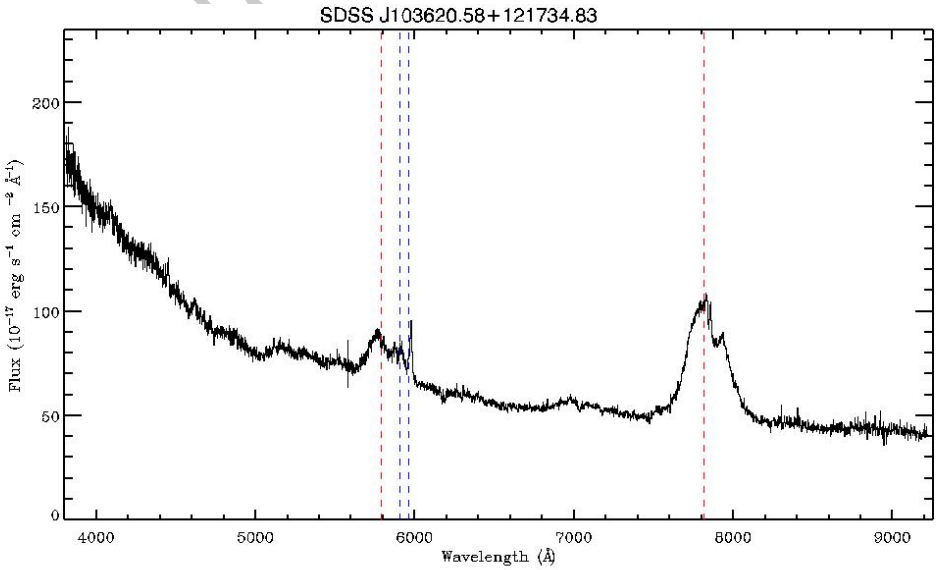

Fig. 25 An example of a "weak-component". The difference between single AGN spectra and such spectra is apparent: the H_α region (at 7800 $\dot{A}$), for example, contains an extra, weaker set of emission line.

The H_α region is a fine example of a "weak-component" twin-peak structure. The primary broad-line constitute of most of the profile, centered approximately at the redshift line, suggesting that this stronger component usually is produced by a more massive AGN. The weaker component is at a slightly higher redshift near $8000\dot{A}$. It is not yet strong enough or at higher velocity separations to resemble a "twin-peak" as in **Fig. 23**, and the result is the appearance of a "sub-peak" on the sides of the primary peak.

In **Fig. 26** we plot a demonstration of how such a "weak-component" spectra may form and evolve with time. The parameters chosen are shown be **Table. 3**

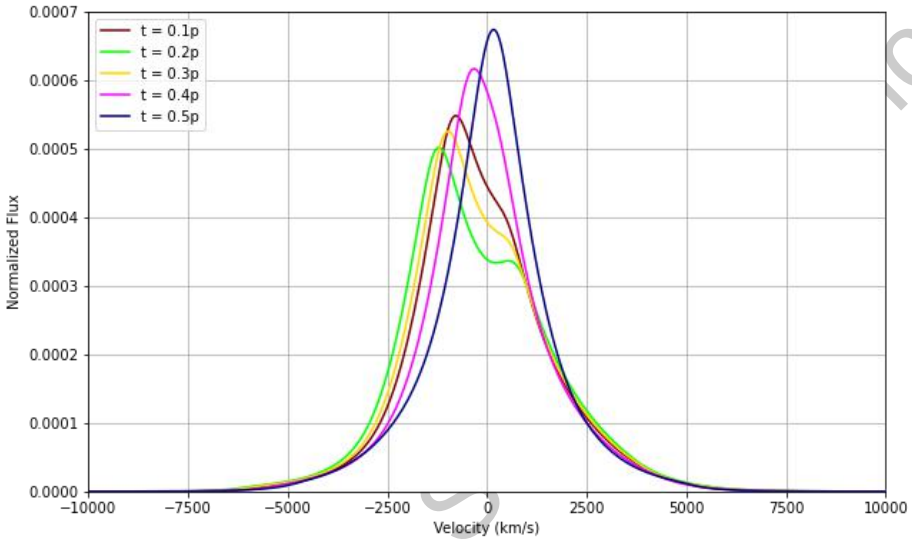

Fig. 26 "Weak-component" spectra. Lines are again plotted with 1/10 of the period. Note that there exist two types of spectra: "Weak-component", and a "velocity-offset" profile we shall discuss later

Parameter	AGN1	AGN2
$\mathbf{a_{in}}$	20 ltdy	10 ltdy
$\mathbf{a_{out}}$	50 ltdy	20 ltdy
$\boldsymbol{\theta_{inc}}$	15	15
$\boldsymbol{\theta_{open}}$	90	90
e	0	0
$\boldsymbol{\omega}$	0	0
$\boldsymbol{\gamma}$	0	0
$\boldsymbol{\beta}$	7	7
$\mathbf{v_{turb}}$	500 km/s	500 km/s
$\mathbf{M_B}$	$10^{7.8}M_{sun}$	$10^{8.1}M_{sun}$

Table 3 List of parameters

The orbital parameters are $a_* = 100\ ltdy, e = 0.3, \omega = 40°, i = 60°$. It can be seen that the shape of the profile is different to that of single-AGNs. Our model has reproduced the small "sub-peak" seen in **Fig. 25**, for example the line $t = 0.2P$. This "sub-peak" does not contribute to another emission peak in the profile, but rather deforms the main peak's profile at the slopes. This feature can sometimes be mistaken for other sets of superimposed emission lines, for example strong iron emission in the $H\beta$ region. It would then be required that this feature exists in all Balmer emission lines; in addition, we would require high S/N spectra in order to remove the possibility of noise hiding the "sub-peak". A more significant feature to observe is the deviation of

the main peak from the center. Single AGN generates profiles peaked more or less centered at 0 km/s, save the rare cases of a highly eccentric orbit. In the absence of twin-peaked profiles, deviation from the measured emission wavelength can suggest the existence of a binary AGN, as the most probable explanation is the velocity offset by Keplerian motion.

Variations of the "Weak-component" profile is less significant than that of the "twin-peak". This is due to the longer period and hence more difficult to observe, as well as the relatively close broad-lines (on the velocity spectrum), which limits variability in magnitude. The time period of orbital motion for the above parameters is 178 years, and hence any variations would be much longer than that of the "twin-peak" profiles. Despite difficulties in observing its variation, however, its profile stands out quite significantly. In **Fig. 27** we present another "weak-component" spectra, this time with our model fit.

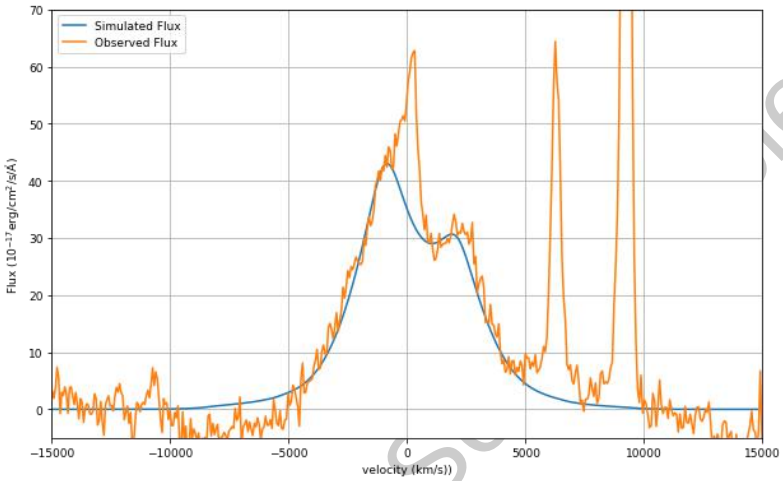

Fig. 27 Fitting of the H_β region J153415.41+303435.45. The parameters are chosen

As seen from the fitted spectra, the profile contains precisely a main peak and a sub-peak, at velocity offset -1000 km/s and 2000 km/s, respectively. It should be noted at such high velocity separation it would be possible to form "twin-peaked" structures; however from the fitting we can see that one peak, the "sub-peak", comes from an AGN much less luminous than its counterpart. Even so, the high velocity separation suggests that it would be possible to observe some variations in the profile due to Keplerian motion.

It can be seen from **Fig. 26** that as time evolves, the "sub-peak" is absorbed into the main profile to resemble a typical broad-line. There is, however, another difference. While the profile $t = 0.4P$ contains only one peak, without any "sub-peaks", it can be categorized as a binary candidate based on its *velocity offset* from the center. As stated before, it would require highly eccentric orbits for single AGNs to achieve this shift, and the best explanation would be that the profile is Doppler shifted (radial velocity). We plot an example of the profile, with $t = 0.6P$ and the same parameter from **Fig. 26**, in **Fig. 28**.

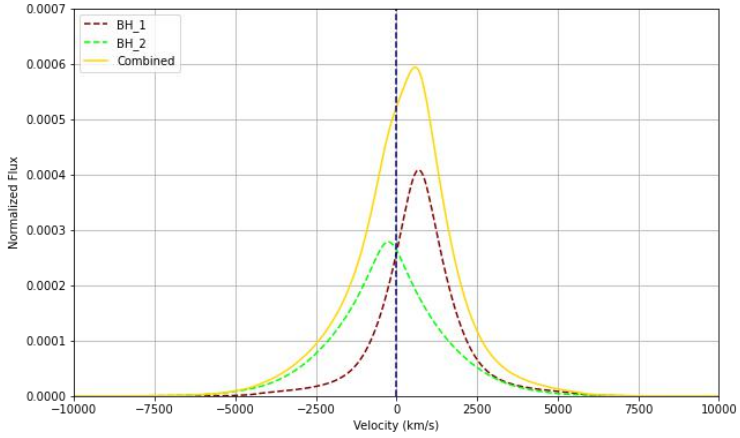

Fig. 28 "Velocity-Offset" binary profile

The most significant feature of this profile is of course the deviation of its peak from the 0 km/s mark. This can be explained by observing the components that makes up the profile (the dashed lines). When the profiles are lined close together, with one weaker than the other, no "sub-peak" is produced, and the result is a skewed profile. It can be seen that the skewness is shown by the different slopes to either side of the peak: the "blue" side of the profile has a more moderate slope while the "red" side shows a high slope. This asymmetricity, coupled along with a Doppler-shifted peak, can help to identify the presence of a binary candidate. It should be warned, however, that in order for identification to be possible the redshift z must be precisely measured, for true deviations from the peak is usually small (<1000 km/s). Incorrect redshifts can mistakenly lead to the identification of AGNs with an eccentric BLR as a binary candidate.

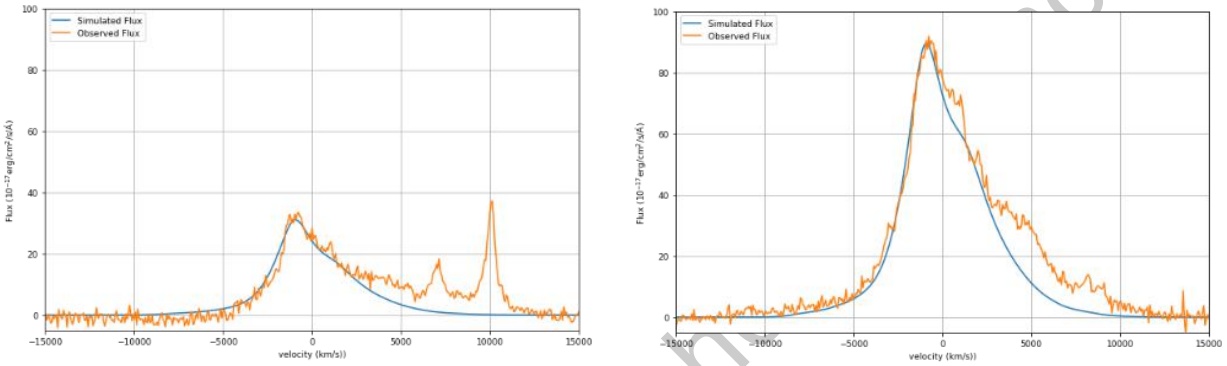

Fig. 29 Fitted spectra for the AGN (system) J001224.02-102226.29. Left: H_β region of the profile. Right: H_α region of the profile. The profiles are fitted with the same parameters; only the weights given are different.

In **Fig. 29** we have fitted the profile for the AGN (system) J001224.02-102226.29, for the strong Balmer lines H_α and H_β. The two profiles are at velocity separation 1100 km/s and -1000 km/s. It can be seen that the modelled profile describes a skewed peak, the "red" slope being gentler than the "blue" slope, which shows a sharp increase in flux. This is because the weaker component is somewhat broader than the main peak, and so the base of the profile is broadened. The system is thought to be a binary system for its peak being shifted by -1000 km/s, in accordance to the results described by our model in **Fig. 28**. The Balmer profiles furthermore follow the same general shape described by our model. In fitting the spectra, we would expect the only parameter difference to be the weights added to each profile. In the case above, H_α emission is relatively stronger in the profile shifted to the right (red-shifted). Its H_β emission is accordingly relatively weaker, suggesting a higher energy level in this AGN.

Parameter	AGN1	AGN2
$\mathbf{a_{in}}$	10 ltdy	50 ltdy
$\mathbf{a_{out}}$	20 ltdy	60 ltdy
$\boldsymbol{\theta_{inc}}$	15	0
$\boldsymbol{\theta_{open}}$	30	70
$\mathbf{e}$	0	0
$\boldsymbol{\omega}$	0	0
$\boldsymbol{\gamma}$	0	0
$\boldsymbol{\beta}$	7	7
$\mathbf{v_{turb}}$	700 km/s	500 km/s
$\mathbf{M_B}$	$10^8 M_{sun}$	$10^8 M_{sun}$

Ratio for H_α	1.07
Ratio for H_β	0.857

Table 4 Parameter list. The "ratio" is calculated as the weight assigned to AGN1, W(1), divided by the weight assigned to AGN2, r = W(1)/W(2)

3.3.3 Selection of Binary Candidates in SDSS and Discussion of Odd Cases

Our work above has summarized some properties of binary AGN spectra. In addition, we have seen how the model can describe various features in binary candidates. Following the properties from the previous section, we will now select a list of possible binary candidates for verification (for example, by observing time-variations). We have obtained a dataset of 1348 AGN spectra from the SDSS spectroscopy database, selected for their high S/N ratio. Of these spectra we manually identify features discussed in the previous two sections, including twin-peaked structures (rare) and "weak-component" spectra, as well as emission lines shifted at a velocity offset relative to the center-of-mass redshift. AGNs holding these features are highly probable binary candidates and hence important for future, follow-up observations. In **Table 5** we include a list of binary AGN candidates, identified based on the results our model has produced. We have also labelled the feature used to identify said spectra as belonging to that of a binary AGN. In particular, SP refers to spectra with "sub-peaks", with deformation of one of the slopes showing a smaller peak. TP refers to the typical case of a twin-peaked spectra, with both peaks visible and prominent. VO refers to "velocity-offset" profile, profiles showing skewed peaks that deviates from their correct redshift.

Name	Plate-MJD-FiberID	z	Category
J135829.57+010908.45	0301-51942-0457	0.2439	SP
J172711.81+632241.85	0352-51789-0639	0.2174	VO
J034042.93-073125.56	0462-51909-0133	0.2165	VO
J121018.35+015405.94	0517-52024-0027	0.2159	SP
J143515.65+023221.55	0535-51999-0582	0.3050	VO
J001224.02-102226.29	0651-52141-0072	0.2281	VO
J093653.84+533126.92	0768-52281-0473	0.2281	VO
J103620.58+121734.83	1600-53090-0363	0.1925	SP
J085632.99+595746.94	1785-54439-0481	0.2830	SP
J130534.49+181932.91	2603-54479-0443	0.1180	SP
J133432.35+171147.02	2606-54154-0581	0.2648	VO+SP
J122630.99+252522.18	2659-54498-0353	0.1336	SP
J140336.43+174136.14	2757-54509-0152	0.2223	TP
J140431.42+213415.44	2784-54529-0027	0.0839	TP
J140315.91+225845.34	2784-54529-0535	0.1606	VO
J222435.29-001103.89	4201-55443-0033	0.0579	VO
J001224.01-102226.51	7169-56628-0344	0.2274	VO
J001247.93-084700.59	7169-56628-0665	0.2204	VO
J225307.36+194234.60	7609-56959-0283	0.2820	SP
J225421.65+211816.22	7609-56959-0850	0.1510	SP
J004319.74+005115.41	7856-57260-0132	0.3090	VO+SP
J075403.60+481428.05	8303-57805-0778	0.2741	SP
J170553.87+455115.30	8535-58019-0892	0.2573	VO
J230803.20-013729.91	9153-58022-0174	0.2022	SP
J013521.27+062548.58	11071-58429-0410	0.1492	VO
J094927.67+314109.94	11379-58438-0592	0.3052	VO

Table 5 List of most confident binary candidates. Candidates marked with asterisk are spectra differing from that of single AGNs yet unexplained by our model, which we have included for later verification.

Of the 26 profiles we identified as being possible binary profiles, only two are marked as being "twin-peaked": J140336.43+174136.14, and J140431.42+213415.44, and their peak structures are not as easily identifiable as in J1536+0441. The rarity of this result suggests that binary systems whose AGNs are close enough to assume a twin-peaked structure are rare. A possible explanation for the lack of twin-peaked structures may be that at this stage of proximity, relativistic effects become significant, and orbital decays may alter the structure of the BLR completely so our model can no longer describe it.

Other candidates are much more common, those identified by their "sub-peak" or "velocity-offset" feature. In our model this is much explained by Keplerian orbits and hence those are very reliable candidates.

We further point out that the AGN J150752.66+133844.50 shows an extremely broad profile (see **Fig. 30**) not identified by our model. The width of the profile cannot be described satisfyingly for a single AGN unless for extremal parameters. Considering **Fig. 18** in **Section 3.1.3**, the profile may be reproduced by a highly inclined, spherical BLR. However, highly inclined AGNs are considered to be Seyfert II galaxies and the broad lines are extinguished, making this choice of parameters physically improbable. Another explanation would be a combination of very broad "twin-peak" binaries, spaced at approximately $\pm 5000\ km/s$, to produce the width of the profile. Such a high velocity separation suggests an extremely short orbital period. If this was indeed a binary candidate, it is suggested that further observations are required to confirm the case, to see if there are any changes to the profile, most notably large magnitude variations.

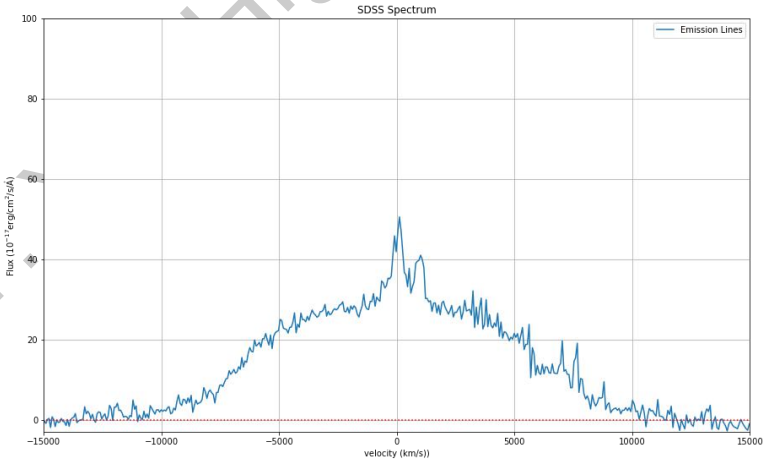

Fig. 30 Profile of J150752.66+133844.50. The dashed line marks the 0 flux emission from the broad-lines (negative values are due to fitting of the continuum data)

We report the AGN (system) J005709.93 + 144610.28 (not included in list) as being a "dual AGN", meaning that the AGN components form a *visual* binary rather than true, gravitationally bound binary systems. This can be seen from the *resolved* emission cores in **Fig. 31**.

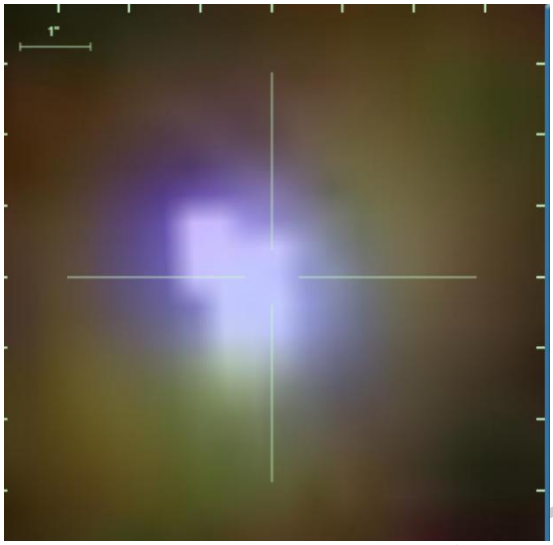

Fig. 31 The spatially resolved cores at an angular separation of approximately 1"

At such a large separation it is improbable that the two cores can form a binary system. Such a "dual-binary" is at redshift z = 0.172, and from this we calculate the separation at this distance to be approximately 3kpc. At such a large separation the two are not yet gravitationally interacting. For reference, the AGN (system) J1536+0441 is thought to be at separation 0.1pc (Boroson & Lauer 2009), with an orbital period of 100 years. As the period is $p \sim a^{1.5}$, even if this were a (weakly) interacting binary, the period would be approximately $5.2 \times 10^8\ yr$. This helps to explain the abnormality of its profile (**Fig. 31**), where the broad H_α and H_β lines contrast greatly with the different structure of the H_γ line.

At such a large separation it is improbable that the two cores can form a binary system. Such a "dual-binary" is at redshift z = 0.172, and from this we calculate the separation at this distance to be approximately 3kpc. At such a large separation the two are not yet gravitationally interacting. For reference, the AGN (system) J1536+0441 is thought to be at separation 0.1pc (Boroson & Lauer 2009), with an orbital period of 100 years. As the period is $p \sim a^{1.5}$, even if this were a (weakly) interacting binary, the period would be approximately $5.2 \times 10^8\ yr$. This helps to explain the abnormality of its profile (**Fig. 31**), where the broad H_α and H_β lines contrast greatly with the different structure of the H_γ line.

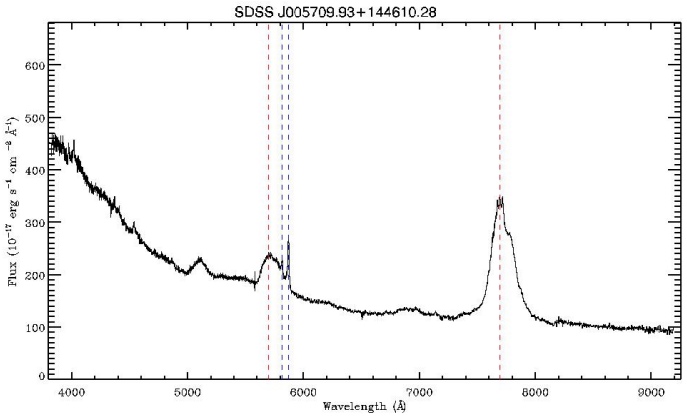

Fig. 32 Profile of the AGN J005709.93 + 144610.28. The different profile structure of the Balmer lines suggests this is not a simple binary system: H_α is "sub-peak" like, H_β is broad and H_γ is sharper.

There are clues to which we can infer about the "dual" binary. The extreme width of the profile can be explained in our model by large velocity separation, however from the resolved cores it can be concluded that the velocity separation must not be due to radial velocity offset, as those are too small to be significant. The velocity separation can be explained by interpreting the resolved cores as freely moving AGN cores, and their appearances as "binary" is purely visual, thus allowing the width of the profile.

4 CONCLUSION

In this paper we have developed a model to simulate the emission-line profile from Seyfert I AGN systems. We have then extended this model to explain and generate profiles for binary AGN systems, by shifting the profiles with a velocity offset. The profiles created were able to match and interpret profiles as being a binary system, suggesting the feasibility of our model to identify binary candidates. Discussions were included for the expected time-variation of the profiles, suggesting time-scales for observing changes in binary profiles. We finally included a list of confident binary candidates that may be verified by further observation (i.e., look for changes described in paper) to be true interacting binaries. We concluded our discussions by pointing out unusual cases and their possible explanations.

The model we have developed follows simply manipulated physics that matches observed spectra extremely well. This suggests that, on a whole, AGNs can be explained fully by theories of simplicity waiting to be found. We have considered and assumed a direct relation between time and mass of the BLR clouds, suggesting that we can sample radial velocity curves generated by Python programs. Our model introduced the BLR model as a ring-like structure, its extent defined by the opening angle θ_{open}. The model constructs the profile by summing over all distances from the core as well as all planes withing the opening angle. We then verified certain parameter constrains based on their effects on the final profile. This greatly limits the parameter space, allowing the generation of binary profiles.

Our achievements can then be summarized as follows:

1. Constructing a feasible model that is able to fully described broad-line structure of single AGN;
2. Successfully reproducing observed broad emission lines of AGNs with our model;
3. Extending our model to be able to generate line profiles of binary blackholes;
4. Identifying key structural and variation features unique to binary spectra;
5. Selecting binary blackhole candidates based on features suggested by our model, yielding 28 high value candidates is sample of 1348 SDSS AGN spectra with high signal-to-noise ratio.

Binary AGNs are a key area of study in astronomy, as they provide valuable data on the evolution of galaxy mergers. It is further thought that gravitational interaction between galaxies

can initiate the fueling of the accretion process, hence providing us insight into the true physical nature of AGNs. The difficulty of observing a binary AGN remains, as they are found at large distances with no apparent visual differences to common. Despite difficulties and inadequate modelling procedures, our model has still produced satisfying results. Our work has greatly narrowed the range of possible candidates that can be verified by further observation. We hope that the future observations are able to verify or reject our selected list of candidates, so that insights may be provided to improve our model. We are confident that by refining our model in the future, the selection of binary AGNs will become more reliable and efficient.

References

1. Boroson, T.A. & Lauer, T.R., 2009. A candidate sub-parsec supermassive binary black hole system. Nature, 458(7234), pp.53–55. Available at: http://dx.doi.org/10.1038/nature07779
2. Boroson, T.A. & Lauer, T.R., 2009. A candidate sub-parsec supermassive binary black hole system. Nature, 458(7234), pp.53–55. Available at: http://dx.doi.org/10.1038/nature07779
3. Eracleous, M. et al., 2012. A LARGE SYSTEMATIC SEARCH FOR CLOSE SUPERMASSIVE BINARY AND RAPIDLY RECOILING BLACK HOLES. The Astrophysical Journal Supplement Series, 201(2), p.23. Available at: http://dx.doi.org/10.1088/0067-0049/201/2/23
4. Ghez, A.M. et al., 1998. High Proper-Motion Stars in the Vicinity of Sagittarius A*: Evidence for a Supermassive Black Hole at the Center of Our Galaxy. The Astrophysical Journal, 509(2), pp.678–686. Available at: http://dx.doi.org/10.1086/306528
5. Gillessen, S. et al., 2009. THE ORBIT OF THE STAR S2 AROUND SGR A* FROM VERY LARGE TELESCOPE AND KECK DATA. The Astrophysical Journal, 707(2), pp.L114–L117. Available at: http://dx.doi.org/10.1088/0004-637x/707/2/l114
6. Graham, M.J. et al., 2015. A possible close supermassive black-hole binary in a quasar with optical periodicity. Nature, 518(7537), pp.74–76. Available at: http://dx.doi.org/10.1038/nature14143
7. Moaz, D. (2007) *Astrophysics in a Nutshell*, Princeton University Press, pp. 94-97,165-170
8. Pancoast, A., Brewer, B.J. & Treu, T., 2014. Modelling reverberation mapping data – I. Improved geometric and dynamical models and comparison with cross-correlation results. Monthly Notices of the Royal Astronomical Society, 445(3), pp.3055–3072. Available at: http://dx.doi.org/10.1093/mnras/stu1809
9. Perryman, M. (2018) *The Exoplanet Handbook*, Cambridge University Press, 2nd Edition
10. Peterson, B. (1997) *Introduction to Active Galactic Nuclei*, Cambridge University Press
11. Storchi-Bergmann, T. et al., 2017. Double-Peaked Profiles: Ubiquitous Signatures of Disks in the Broad Emission Lines of Active Galactic Nuclei. The Astrophysical Journal, 835(2), p.236. Available at: http://dx.doi.org/10.3847/1538-4357/835/2/236
12. Wang, X.-W. & Zhou, H.-Y., 2012. DUAL ACTIVE GALACTIC NUCLEI: DEPROJECTING THE BINARY CORES. The Astrophysical Journal, 757(2), p.124. Available at: http://dx.doi.org/10.1088/0004-637x/757/2/124
13. Zhang, S. et al., 2019. SDSS J153636.22+044127.0 and Its Analogs: Shocked Outflows, Not Active Binary Black Holes. The Astrophysical Journal, 877(1), p.33. Available at: http://dx.doi.org/10.3847/1538-4357/ab1aa3

Acknowledgement

This study originated from readings regarding Quasars and Active Galactic Nuclei. Current studies are limited in the fields of Active Galactic Nuclei in binary orbits, while such systems are important in the studying the development of galaxy systems. As the emission-line profile of Active Galactic Nuclei demonstrate different characteristic as to normal galaxy absorption systems, this paper focuses on studying the features of the emission profile of binary AGN.

Dr. Jiang Peng acts as the writer's director teacher. Dr. Jiang provided professional background and scientific knowledge background prior to the initiation of the project. These include leading the writer through journals and papers to gain a sound understanding of previous work as well as gaps in the area I have chosen. Dr. Jiang provided useful insights and improvements to the coded simulation and model. Dr. Jiang had also helped to review the writer's paper, in correcting technical details and format. The writer is sincerely grateful for the support and help from Dr. Jiang Peng.

This paper was completed by the writer and the writer alone. All simulation processes and codes are written by the writer, with directions and help from Dr. Jiang. The writer pledges that the submitted work and paper is completed under the guidance of the director teacher. It is understood that our paper does not contain any work completed by others, or other published work not listed in the reference section. The writer understands that should any false claims be made, the writer will take full responsibility.